JCB Journal of Cell Biology

ARTICLE

Mechanical stress impairs pheromone signaling via Pkc1-mediated regulation of the MAPK scaffold Ste5

Frank van Drogen[1*], Ranjan Mishra[1*], Fabian Rudolf[1], Michal J. Walczak[2], Sung Sik Lee[1,3], Wolfgang Reiter[4], Björn Hegemann[1], Serge Pelet[5], Ilse Dohnal[4], Andres Binolfi[6], Zinaida Yudina[1], Philipp Selenko[6], Gerhard Wider[2], Gustav Ammerer[4], and Matthias Peter[1]

Cells continuously adapt cellular processes by integrating external and internal signals. In yeast, multiple stress signals regulate pheromone signaling to prevent mating under unfavorable conditions. However, the underlying crosstalk mechanisms remain poorly understood. Here, we show that mechanical stress activates Pkc1, which prevents lysis of pheromone-treated cells by inhibiting polarized growth. In vitro Pkc1 phosphorylates conserved residues within the RING-H2 domains of the scaffold proteins Far1 and Ste5, which are also phosphorylated in vivo. Interestingly, Pkc1 triggers dispersal of Ste5 from mating projections upon mechanically induced stress and during cell–cell fusion, leading to inhibition of the MAPK Fus3. Indeed, RING phosphorylation interferes with Ste5 membrane association by preventing binding to the receptor-linked Gβγ protein. Cells expressing nonphosphorylatable Ste5 undergo increased lysis upon mechanical stress and exhibit defects in cell–cell fusion during mating, which is exacerbated by simultaneous expression of nonphosphorylatable Far1. These results uncover a mechanical stress–triggered crosstalk mechanism modulating pheromone signaling, polarized growth, and cell–cell fusion during mating.

Introduction

Interplay between signaling networks determines proper regulation of cell growth, survival, and fate. In the budding yeast *Saccharomyces cerevisiae*, many signaling components have been identified and studied at the molecular and mechanistic levels (Brent, 2009; Alvaro and Thorner, 2016), but the dynamic interactions required to temporally and spatially orchestrate appropriate cellular responses remain poorly understood. One such case is the yeast pheromone response pathway, which is activated in a cell cycle–dependent manner in haploid cells upon contact with a partner of opposite mating type. Pheromone signaling is inhibited by CDK activity and thus restricted to the G1 phase of the cell cycle when both partners have an equal amount of DNA, assuring genomic integrity (Strickfaden et al., 2007). In addition, other intra- and extracellular stress signals impinge on the mating reaction to avoid cell lysis under conditions unfavorable for mating and cell–cell fusion. For example, signaling through the high-osmolarity glycerol pathway down-regulates the pheromone response pathway (Yamamoto et al., 2010; Vaga et al., 2014). Yeast mating thus offers an attractive system to study signal integration in cell fate determination, as multiple and at times opposing signaling inputs can be combined.

Pheromone signaling induces G1 cell cycle arrest, cell polarization, and initiation of a cell–cell fusion transcriptional program (Dohlman and Slessareva, 2006). All three responses are orchestrated by the scaffolds Ste5 and Far1, which function as assembly platforms and comprise important regulatory nodes that allosterically modulate signaling output (Ferrell and Ciprich, 2003). Mating pathway activation is triggered by pheromones binding to dedicated receptors, which leads to dissociation of the Gβγ heterodimer (Ste4–Ste18) from the α-subunit (Gpa1) of the heterotrimeric G protein. Ste5 and Far1 bind the released Gβγ complex through their RING-H2 domains at the plasma membrane. Ste5 membrane association further requires cooperative effects of the pleckstrin homology (PH) domain and the plasma membrane binding motif (PM) domain to increase cell membrane affinity (Winters et al., 2005). Pheromone signaling is down-regulated by negative feedback

[1]Institute for Biochemistry, ETH Zürich, Zürich, Switzerland; [2]Institute of Molecular Biology and Biophysics, ETH Zürich, Zürich, Switzerland; [3]Scientific Center for Optical and Electron Microscopy, ETH Zürich, Zürich, Switzerland; [4]Department of Biochemistry, Max F. Perutz Laboratories, University of Vienna, Vienna, Austria; [5]Department of Fundamental Microbiology, University of Lausanne, Lausanne, Switzerland; [6]Department of Nuclear Magnetic Resonance–Supported Structural Biology, Leibniz Institute of Molecular Pharmacology, Berlin, Germany.

*F. van Drogen and R. Mishra contributed equally to this paper; Correspondence to Frank van Drogen: vafrank@ethz.ch; Matthias Peter: matthias.peter@bc.biol.ethz.ch; F. Rudolf's present address is Dept. of Biosystems Science and Engineering, ETH Zürich, Basel, Switzerland; M.J. Walczak's present address is Captor Therapeutics Ltd., Wroclaw, Poland; I. Dohnal's present address is BIOMIN Research Center, Tulln, Austria.

through the MAPK Fus3 (Choudhury et al., 2018; Repetto et al., 2018) and CDK1-mediated phosphorylation of multiple sites flanking the PM domain (Oehlen and Cross, 1994; Strickfaden et al., 2007) by electrostatic exclusion with the negatively charged head groups of the phospholipids (Strickfaden et al., 2007).

Membrane-bound Ste5 associates with and activates a MAPK module composed of Ste11, Ste7, and the MAPKs Fus3 and Kss1, while Far1 binds and activates the Cdc42 exchange factor Cdc24 to direct cell polarity (Dohlman and Slessareva, 2006). The PAK-like kinase Ste20 phosphorylates Ste11 in a Cdc42-dependent manner. Ste11 then activates Ste7, which in turn doubly phosphorylates Fus3 and Kss1. Activated Fus3 and Kss1 phosphorylate cytoplasmic and cell membrane–tethered targets, including Ste18 and Far1, to promote cell cycle arrest and translocate into the nucleus, activating a specific transcriptional program.

Polarized growth toward the mating partner and the subsequent cell–cell fusion events require spatial cell wall remodeling that renders cells vulnerable to lysis (Zarzov et al., 1996). Upon cell wall stress, Pkc1 is activated, which in turn triggers a MAPK cascade resulting in activation of the MAPK Mpk1 (Slt2; Levin, 2011) to reinforce cell wall synthesis (Smits et al., 1999). Pkc1 is also activated in mechanically stressed cells and prevents cell lysis at least in part by inhibiting actin-driven polarized growth (Delarue et al., 2017; Mishra et al., 2017). Indeed, Mpk1 pathway components are actively recruited to shmoo tips by interacting with the scaffold protein Spa2 (van Drogen and Peter, 2002), and *mpk1Δ* cells show increased lysis upon exposure to pheromones (Merlini et al., 2013; Engelberg et al., 2014).

Here, we show direct pheromone pathway modulation by the cell wall integrity (CWI) pathway upon mechanical stress. We found that physical pressure activates Pkc1, which in turn prevents Ste5 accumulation at shmoo tips. Molecular analysis revealed that phosphorylation of specific sites in the RING-H2 domains of Ste5 and Far1 interfere with their binding to Gβγ heterodimers, thereby inhibiting Fus3 activity. In the absence of this mechanism, cell viability is reduced due to increased lysis during pheromone-induced polarized growth and cell–cell fusion. Thus, timely inactivation of pheromone signaling by regulating Gβγ-mediated membrane association of the scaffold proteins Ste5 and Far1 is part of a Pkc1-dependent crosstalk mechanism to prevent cell lysis in response to mechanical stress and cell wall remodeling during cell–cell fusion.

Results

Mechanical stress inhibits the pheromone response pathway in a Pkc1-dependent manner

Previously, we have shown that mechanical stress activates Pkc1 to protect cells from lysis partially by inhibiting polarized growth (Mishra et al., 2017). Indeed, inhibition of Pkc1 with cercosporamide, or overexpression of a dominant-negative Pkc1 allele ($Pkc1^{K853R}$; Watanabe et al., 1994), increased lysis of pheromone-treated cells exposed to mechanical stress (Fig. 1, A–C). Because the MAPK Fus3 promotes polarized growth and shmoo formation, we used the Fus3 SKAR (synthetic kinase activity relocation) reporter (Durandau et al., 2015) to assess whether mechanical stress inhibits Fus3 activity. As expected, the SKAR reporter was mainly cytoplasmic in pheromone-treated cells but showed nuclear accumulation with mechanical pressure, implying that Fus3 activity is reduced in response to mechanostress (Fig. 1 D). Cercosporamide prevented Fus3 inhibition, and phenotypic analysis revealed that those cells displaying high Fus3 activity lyse (Fig. 1 E). Additionally, we quantified mechanostress induced lysis of cells expressing a NaPP1-inhibitable Fus3 mutant protein. Indeed, Pkc1-inhibited cell lysis was suppressed by simultaneous addition of NaPP1 (Fig. 1 F), indicating that Pkc1-dependent Fus3 inhibition protects cells from mechanostress induced lysis during mating. This Pkc1-dependent crosstalk to the pheromone pathway was unlikely to be caused by off-target effects of cercosporamide (Fig. S1). Surprisingly, cells lacking the MAPK Mpk1 were less prone to lyse than cercosporamide-treated cells (Fig. 1 G), implying that unknown Pkc1 targets must exist to protect cells from mechanostress-induced lysis in response to pheromones. To understand this crosstalk, we examined Ste5 localization upon mechanical stress. While triple Venus (tV)–tagged Ste5 (Ste5-tV) accumulated at shmoo tips in the absence of stress, Ste5-tV was dispersed upon mechanical pressure (Fig. 1 H), which activates both Pkc1 and Mpk1 (Fig. S2, A and B). Ste5 dispersal was blocked by addition of cercosporamide primarily by an Mpk1-independent mechanism (Figs. 1 H and S2 C), implying that Pkc1 may directly regulate membrane association of Ste5. Indeed, Ste5 dispersal was mimicked by expression of a dominant-active Pkc1 ($Pkc1^{R398A}$; Fig. S2 D). Furthermore, expression of $Pkc1^{R398A}$ before pheromone treatment resulted in failure to recruit Ste5 and form shmoos (Fig. S2, E and F). In contrast, cells expressing a weakly constitutive allele of Bck1 (Bck1-20) responded normally to pheromone (Fig. S2 G). Together, these results imply that Pkc1 interferes with pheromone response, likely by preventing membrane association of Ste5 by an Mpk1-independent mechanism (Fig. 1 I).

Ste5 and Far1 are phosphorylated in their RING-H2 domain by Pkc1

We mapped Ste5 phosphorylation sites by tandem mass spectrometry (MS) analysis in cells exposed to α-factor. We purified Ste5-HTB under denaturing conditions, and enriched phosphopeptides using TiO_2. This analysis identified over 40 Ste5 phosphorylation sites (Figs. 2 A and S3 and Table S1), among them several previously described or predicted sites, confirming that Ste5 is a major hub for regulation (Choudhury et al., 2018; Repetto et al., 2018). Interestingly, Ste5 was also phosphorylated on S185 close to the first pair of finger cysteine residues within its RING-H2 domain (Figs. 2 A and S3 A and Table S1). Sequence analysis indicates that the corresponding serine and the surrounding residues are largely conserved in Ste5-containing yeast species, and similar phosphorylatable residues are also found in the Far1 RING-H2 domain (Fig. 2 A). MS/MS analysis of purified Far1 confirmed that S210 and possibly also S208 and S211 in its RING-H2 domain were phosphorylated in cells exposed to α-factor (Figs. 2 A and S3 B and Table S2). The charged residues surrounding Ste5 S185 with downstream lysine residues do not conform to a MAPK consensus site but rather

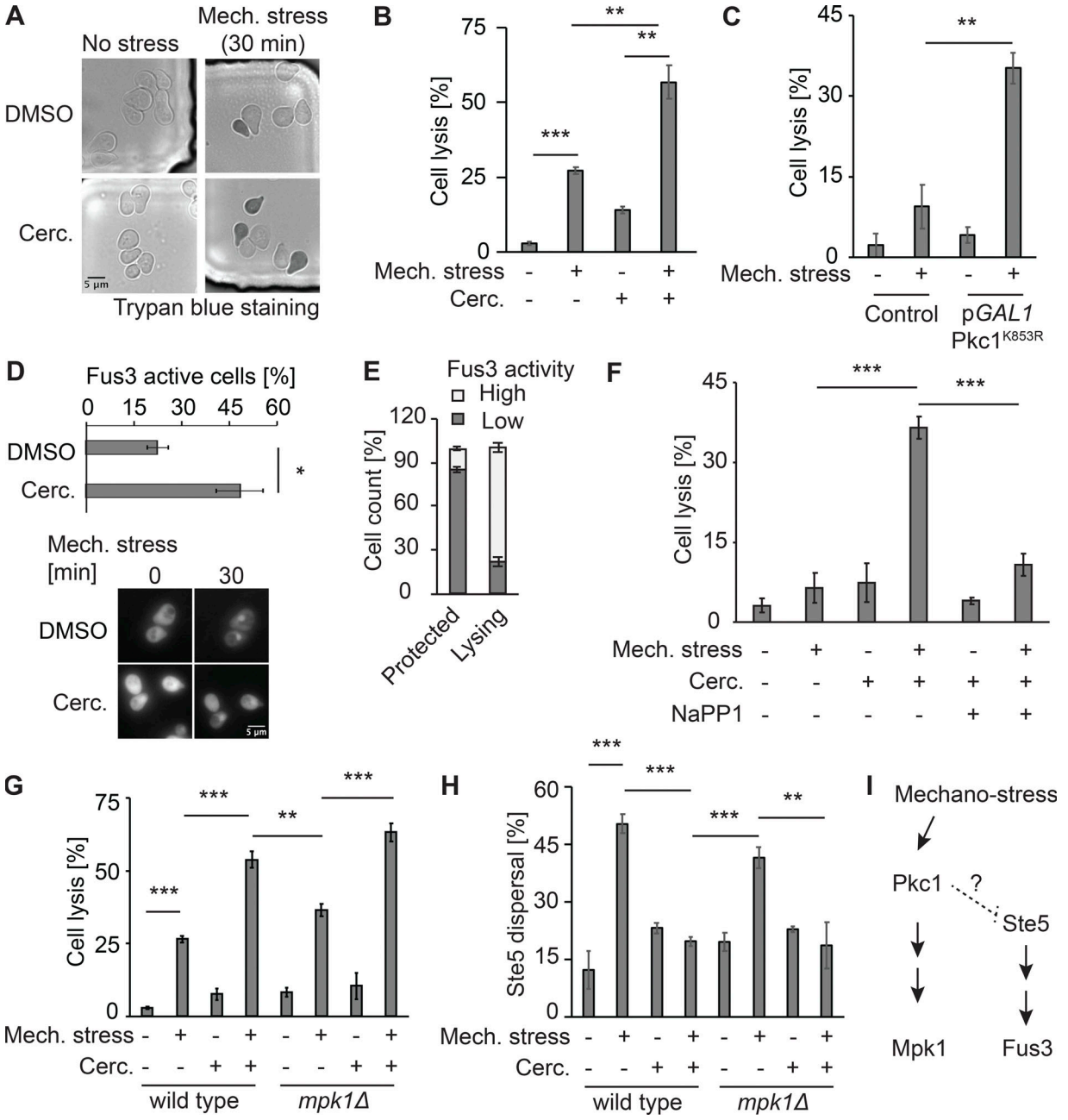

Figure 1. **Pkc1 protects cells from lysis upon mechanostress during pheromone exposure through inhibition of the mating pathway. (A)** Haploid mating-type **a** WT cells were exposed to α-factor for 100 min, followed by 15-min pretreatment with DMSO or 7.5 µM of the Pkc1 inhibitor cercosporamide (cerc.). Then, mechanostress or no stress was applied for 30 min. Lysis of shmooing cells was visualized by phase-contrast microscopy and staining with Trypan blue dye. **(B)** Quantification of cell lysis in shmooing WT cells, treated as in A; >150 cells in at least three independent experiments were quantified for each condition and shown as percentage of lysed cells. Error bars indicate SEM, and significance was determined by *t* test (*, P ≤ 0.05; **, P ≤ 0.01; ***, P ≤ 0.001). **(C)** Quantification of cell lysis in shmooing WT cells harboring or not (control) a plasmid expressing dominant-negative Pkc1 (Pkc1^{K853R}) from the inducible GAL1 promoter. Cells growing in log phase in 2% raffinose were induced with 2% galactose for 2 h followed by exposure to α-factor for 100 min. Mechanostress was applied and cell lysis analyzed as described in B. **(D)** WT cells expressing the Fus3 SKAR and Hta2-CFP reporters were treated with pheromone and 7.5 µM cercosporamide (cerc.) as in A. Nuclear accumulation of the Fus3 SKAR reporting Fus3 activity after 30 min of mechanostress was monitored microscopically and quantified in ≥150 cells in three independent experiments. Error bars indicate SEM, and significance was determined by a *t* test (*, P ≤ 0.05). Representative images before and after mechanostress are shown below. **(E)** WT cells expressing the Fus3 SKARS and Hta2-CFP reporters were treated with pheromone and subsequently with 7.5 µM cercosporamide (cerc.) as described in A, and Fus3 activity was quantified in lysing and protected cells. Cells failing to relocalize the reporter to the nucleus under mechanostress were scored as high Fus3 activity; ≥150 cells were analyzed for each condition in three independent experiments and are shown as percentage of high or low Fus3 activity. Error bars indicate SEM. Note that cells unable to down-regulate Fus3 activity are prone to cell lysis. **(F)** WT cells expressing the chemically inhibitable Fus3-as allele from the endogenous locus were treated with α-factor for 100 min followed by pretreatment with 7.5 µM cercosporamide (cerc.) and 5 µM NaPP1. Then mechanostress was applied. Lysis of ≥150 pheromone-responsive cells was scored for each condition in three independent experiments and is shown as percentage of lysed cells. Error bars indicate SEM, and significance was determined by a *t* test (***, P ≤ 0.001). **(G)** Quantification of cell lysis upon mechanostress in WT or *mpk1Δ* cells treated as in B. At least 150

cells in at least three independent experiments were analyzed for each condition and are shown as percentage of lysed cells. Error bars indicate SEM, and significance was verified by a *t* test (**, P ≤ 0.01; ***, P ≤ 0.001). Genetic background and growth conditions in this experiment are the same as in B, and thus, the data for the WT conditions were combined. **(H)** Cells expressing Ste5-tV under its endogenous promotor in WT or *mpk1Δ* cells were treated as in A, and Ste5-tV was visualized microscopically in microfluidic chips during 30 min of mechanostress. Loss of Ste5-tV at shmoo tips was quantified in ≥150 cells for each condition in at least three independent experiments, and shown as percentage of cells with dispersed Ste5 localization. Error bars indicate SEM and significance was validated by a *t* test (**, P ≤ 0.01; ***, P ≤ 0.001). **(I)** Pkc1-dependent signaling protects mating cells against mechanostress. Pkc1 triggers loss of Ste5 from shmoo tips by an Mpk1-independent mechanism, leading to reduced Fus3 activity.

resemble motifs phosphorylated by Pkc (Kreegipuu et al., 1998). Due to the unfortunate physical properties of this particular phospho-peptide, we failed to establish selected reaction monitoring assays to reliably quantify S185 phosphorylation. While we could detect the phosphorylated S185-containing peptide in pheromone-treated WT and *ste7Δ* cells, the signal was too low to allow robust quantification across different conditions. Therefore, we were unable to determine whether S185 phosphorylation depends on Pkc1 or mechanical stress in vivo. We thus tested whether these serine residues in Ste5 and Far1 could be phosphorylated by Pkc1 in vitro. Indeed, *Escherichia coli*–expressed 6His-RING-H2 fragments of Ste5 (amino acids 149–238) and Far1 (amino acids 173–261) were phosphorylated by GST-Pkc1 affinity purified from yeast extracts and immobilized on GST beads (Fig. 2 B). To confirm that Pkc1 phosphorylates S185, we performed in vitro phosphorylation assays using either WT ($Ste5^{149–238}$) or nonphosphorylatable ($Ste5^{149–238\ S185A}$) RING-H2 fragments of Ste5 and analyzed the phosphorylation status by nuclear magnetic resonance (NMR). Indeed, a new peak was identified in the ^{1}H-^{15}N correlation spectrum upon incubation with yeast extract (Fig. 2, C and D) or purified *Xenopus laevis* Pkc1δ (Fig. S4). This peak was absent when the $Ste5^{149–238\ S185A}$ mutant protein was used as a substrate (Fig. 2 E) or when the kinase assays were performed in the presence of cercosporamide (Figs. 2 F and S4). No additional peaks were detected when the $Ste5^{149–238}$ fragment was incubated with Pkc1, indicating that S185 is the dominant phosphorylation target in the RING-H2 domain.

To test whether Pkc1 and Ste5 directly interact in vivo, we used the M-track protein–protein proximity assay (Zuzuarregui et al., 2012; Brezovich et al., 2015) designed to capture short-lived interactions. Ste5 was tagged with the active enzymatic domain of the murine histone lysine methyltransferase Suv39 (HKMT-myc). Pkc1 was fused to the prey sequence protA-H3, harboring a histone H3 peptide sequence that becomes permanently methylated by Ste5-HKMT-myc upon close proximity. Indeed, as shown in Fig. 2 G, Pkc1 and Ste5 showed M-track proximity signals that increased with extended times of α-factor treatment, indicating a physical interaction between the proteins. We conclude that Pkc1 physically interacts with Ste5 at shmoo tips and directly phosphorylates S185 in its RING-H2 domain in in vitro experiments.

Pkc1-dependent phosphorylation of Ste5 inhibits signaling

We examined Ste5 S185 function in vivo using the nonphosphorylatable ($Ste5^{S185A}$) and phosphomimetic ($Ste5^{S185D}$) versions of GFP-tagged Ste5. Although proteins are expressed at comparable levels (Fig. 3 A), *ste5Δ* cells expressing $Ste5^{S185D}$ were unable to arrest their cell cycle in response to pheromone, while the halo in *ste5Δ* cells expressing $Ste5^{S185A}$ was similar in size when compared with WT controls (Fig. 3 B). After α-factor exposure, *ste5Δ* cells harboring untagged WT Ste5 or $Ste5^{S185A}$ strongly induced expression of the quadruple Venus (qV) fluorescence reporter expressed from the FIG1 promoter (pFIG1-qV), a bona fide Ste12 target, while cells expressing $Ste5^{S185D}$ did not induce even after prolonged exposure (Fig. 3 C). These results suggest that phosphorylation of Ste5 at serine 185 interferes with pheromone signaling in vivo.

We also analyzed WT Far1 and the corresponding nonphosphorylatable $Far1^{3A}$ (S208A, S210A, and S211A) and the phosphomimetic $Far1^{3E}$ (S208E, S210E, and S211E) versions for their ability to polarize cells toward artificial pheromone gradients. While WT and both Far1 mutants were able to arrest the cell cycle as expected, $Far1^{3E}$ exhibited impaired orientation function (Fig. 3 D), which is known to require an intact RING-H2 domain (Lee et al., 2012; Hegemann et al., 2015). Taken together, we conclude that phosphorylation of the RING-H2 domain inhibits Ste5 and Far1 function and renders the scaffolds signaling incompetent in vivo.

Phosphorylation of Ste5 S185 abolishes its interaction with Gβγ

We next investigated Pkc1-mediated Ste5 inhibition. Ste5 is recruited to the plasma membrane by binding to Gβγ through its RING-H2 domain (Whiteway et al., 1995), as well as by interactions between the PM domain and membrane-bound phospholipids (Strickfaden et al., 2007). While GFP-tagged WT Ste5 and the $Ste5^{S185A}$ mutant accumulated at tips of mating projections in WT cells (Fig. 4 A), the phospho-mimicking GFP-$Ste5^{S185D}$ mutant protein was absent from shmoo tips and instead was cytoplasmic. To corroborate these data, we compared the membrane recruitment kinetics of WT and mutant GFP-Ste5 expressed in cells exposed to pheromones (Fig. 4 B; Colman-Lerner et al., 2005). WT and the nonphosphorylatable $Ste5^{S185A}$ mutant showed indistinguishable membrane recruitment kinetics with a fast initial phase followed by a moderate decline due to negative feedback regulation (Yu et al., 2008). In contrast, no membrane recruitment was observed for GFP-$Ste5^{S185D}$, even during early stages, indicating defective initial recruitment. If the membrane recruitment defect is solely responsible for the signaling defect of the $Ste5^{S185D}$ mutant, then its artificial recruitment to the cell membrane should be sufficient to restore signaling (Pryciak and Huntress, 1998). Indeed, pFIG1-qV reporter expression was restored in *ste5Δ* cells expressing a fusion construct from the estradiol-inducible *GAL* promoter of $Ste5^{S185D}$ with a constitutive transmembrane domain (TMD; Fig. 4 C). Taken together, we conclude that phosphorylation of serine 185 in the RING-H2 domain regulates membrane recruitment of Ste5.

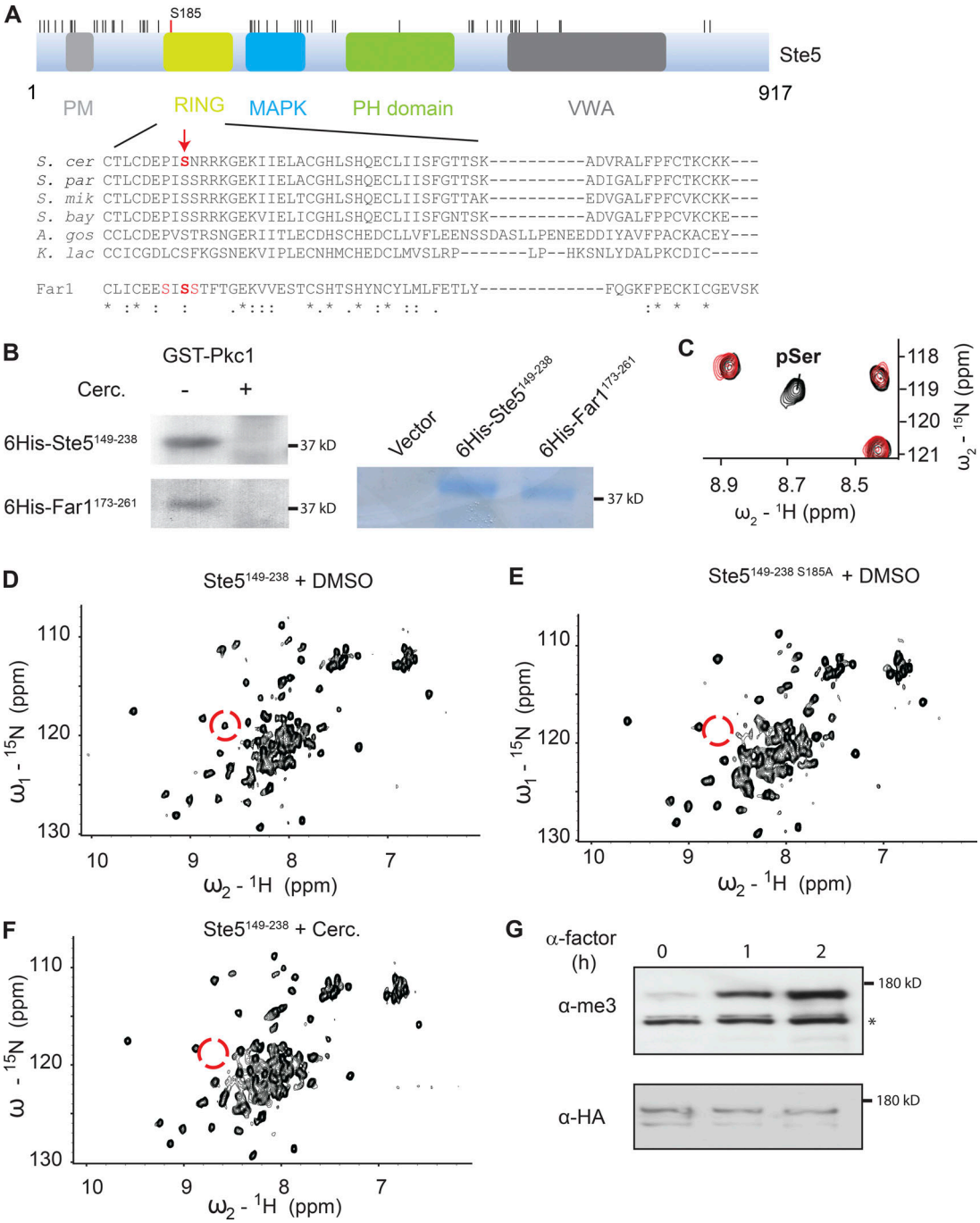

Figure 2. **Serine 185 within the RING-H2 domain of Ste5 is phosphorylated by Pkc1. (A)** Schematic of Ste5 functional domains. MAPK, MAPK docking site; VWA, von Willebrand factor type A domain. Phosphorylated sites identified by MS analysis (localization probability >0.75 according to MaxQuant) in cells exposed to α-factor after phosphopeptide enrichment on a TiO_2 column are indicated by tick marks. The RING domain sequence is aligned with those of different yeast Ste5 proteins and the RING domain of *S. cerevisiae* Far1. Ser^{185} of *S. cerevisiae* is indicated in bold red and conserved in other yeast species. An analogous serine residue (Ser^{210}) located within the Far1 RING domain (bold red) is also phosphorylated, together with two lower confidence sites (red; Ser^{208} and Ser^{211}). **(B)** Recombinant 6His-tagged Ste5- and Far1-RING-H2 fragments were incubated for 30 min at 30°C with GST-Pkc1 purified from yeast extracts containing γ^{32}P-ATP with (+) or without (–) 30 µM cercosporamide (cerc.). Phosphorylated proteins were visualized by autoradiography. An aliquot of purified Ste5- and Far1-RING-H2 fragments were separated by SDS-PAGE and stained with Coomassie blue. The bar points to the 35-kD size marker. **(C–F)** In vitro kinase assays using either WT or the nonphosphorylatable S185A mutant RING-H2 domain with amino acids 149–238 of Ste5 ($Ste5^{149–238}$) as a substrate and incubated as indicated with yeast extracts in the absence (DMSO) or presence of cercosporamide were analyzed by 600 MHz ^{1}H-^{15}N correlation NMR spectra (SOFAST HMQC; Schanda et al., 2005). The resonance position of the phosphorylated Ser185 amide group is magnified in C and highlighted in the dashed circle in D–F. The spectra in C are an overlay of the Ste5-RING-H2 fragment incubated with (black) or without (red) Pkc1. **(G)** M-track protein–protein proximity assays using extracts of cells expressing HKMT-myc–tagged Ste5 (bait) and protA-H3–tagged Pkc1 (prey). Cells were treated with α-factor for the times indicated (hours). Proximity signals were detected by Western blotting using an antibody against triple-methylated lysine of histone H3 (α-me). Loading was controlled via a hemagglutinin epitope embedded in the protA-H3 tag (α-HA). The asterisk marks an unspecific band.

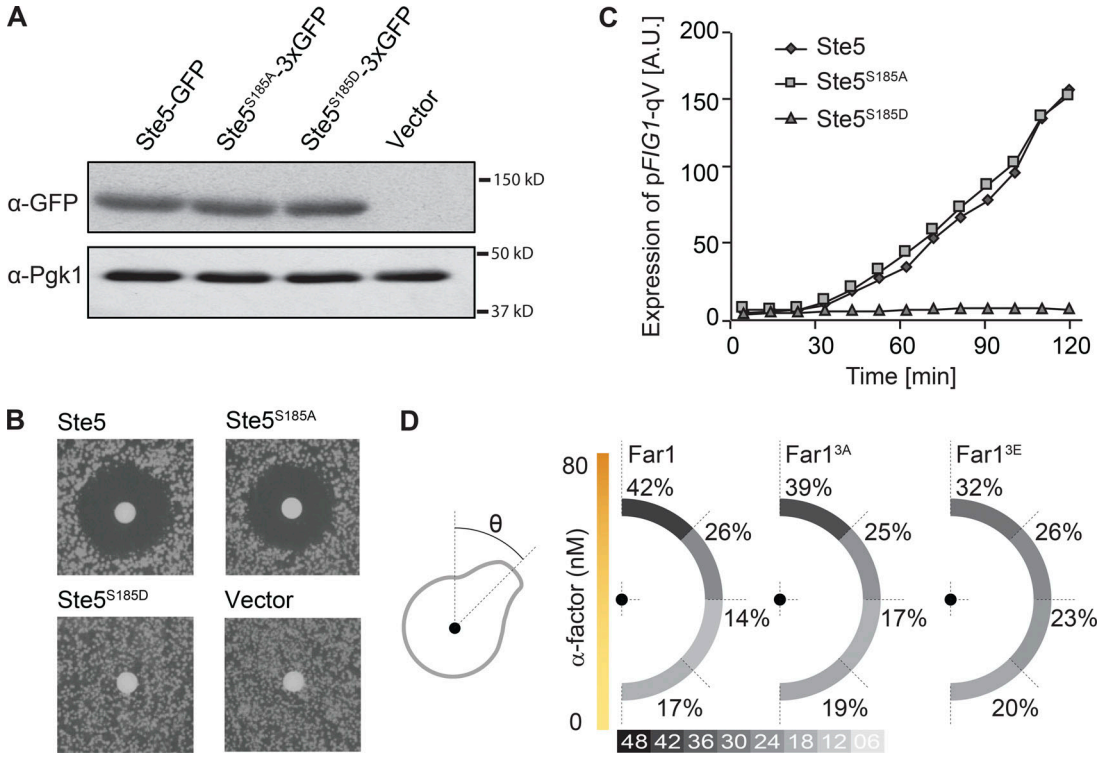

Figure 3. **Phosphorylation of the RING-H2 domains of Ste5 and Far1 inhibits signaling and oriented cell polarity. (A)** Extracts prepared from *ste5Δ* cells expressing 3xGFP-tagged WT Ste5, nonphosphorylatable Ste5^{S185A}, or phospho-mimicking Ste5^{S185D} or harboring an empty control plasmid were analyzed by immunoblotting using anti-GFP antibodies. Pgk1 controls equal loading. **(B)** Halo assays were used to assess cell cycle arrest in response to α-factor for *ste5Δ* cells expressing Ste5 and control constructs as in A. **(C)** Pheromone-dependent gene expression of *ste5Δ* cells harboring a FIG1-qV reporter and the indicated WT Ste5 (diamond), Ste5^{S185A} (square), or Ste5^{S185D} (triangle) was determined by FACS analysis and plotted in arbitrary units at the times indicated (minutes) after α-factor addition. **(D)** Microfluidic chambers generated a 0–80-nM α-factor gradient. The angle of the polarity site with respect to the α-factor gradient (schema) was measured for *far1Δ* strains expressing WT Far1, nonphosphorylatable Far1^{3A}, or phospho-mimicking Far1^{3E}. Results are expressed as percentages and binned into 45° incremental distances (Hegemann et al., 2015).

We next used yeast two-hybrid and in vitro binding assays to examine whether phosphorylation of the RING-H2 domains of Far1 regulates its interaction with free Gβγ. While WT Far1 and the Far1^{3A} mutant readily interacted with Ste4 by two-hybrid assay, binding to phospho-mimicking Far1^{3D} was diminished (Fig. S5, A and B). Likewise, much less 6-His-Ste5^{S185D} was retained on immobilized GST-Ste4 than WT (Fig. 4 D), suggesting that phosphorylation of S185 interferes with binding of Ste5 to Gβγ in vitro. We then performed NMR titration experiments using isotopically labeled (^{15}N) Ste5 RING-H2 domain with unlabeled Gβγ (Ste4–Ste18) purified from yeast (Fig. 4 E), which allows fast and robust assessment of binding partners. Overlaying the NMR spectra of the unphosphorylated RING-H2 domain and the WT RING-H2 domain (Fig. 4 E, black peaks) overtitrated with Gβγ (red peaks) reveals distinctive patterns that indicate binding. Increase of total peak number from ∼90 (black) to ∼170 (red) is consistent with the observation that Ste5 undergoes asymmetric oligomerization while binding to Ste4 (Inouye et al., 1997), although it is unknown whether the asymmetric RING-H2 oligomer is bound to a single Ste4–Ste18 complex or to two complexes that are linked by the homodimerizing GST moiety. The low protein concentrations used for this in vitro assay (10 µM Ste5 and 30 µM Gβγ) and the substantial level of spectral rearrangements imply that the interaction occurs with nanomolar affinity. Analogous titrations with nonphosphorylatable S185A RING-H2 mutant domain similarly showed a specific interaction with Gβγ, although the perturbations were less pronounced (Fig. 4 E, middle panel), indicative of reduced affinity compared with the WT control. Importantly however, no changes in peak positions were detected when titrating Gβγ and the S185D RING-H2 mutant (right panel), demonstrating that the phospho-mimicking mutant protein fails to interact with Gβγ. We were able to assign ∼80% of the peaks in the [^{1}H,^{15}N]-HSQC spectra. This allowed deducing a structural model of the Ste5 RING-H2 domain, comprising three β-strands and two α-helices positioned by the two Zn^{2+} ions that are coordinated by the conserved cysteine and histidine residues (Fig. S5 C). The S185 residue is located between the two N-terminal β-strands, and its phosphorylation could either directly or indirectly regulate Gβγ binding as part of the binding motif or by inducing a conformational change. The NMR-based analysis provides strong evidence that phosphorylation of Ste5 at S185 regulates its interaction with Gβγ and thereby inhibits signaling by preventing membrane recruitment of the scaffold protein.

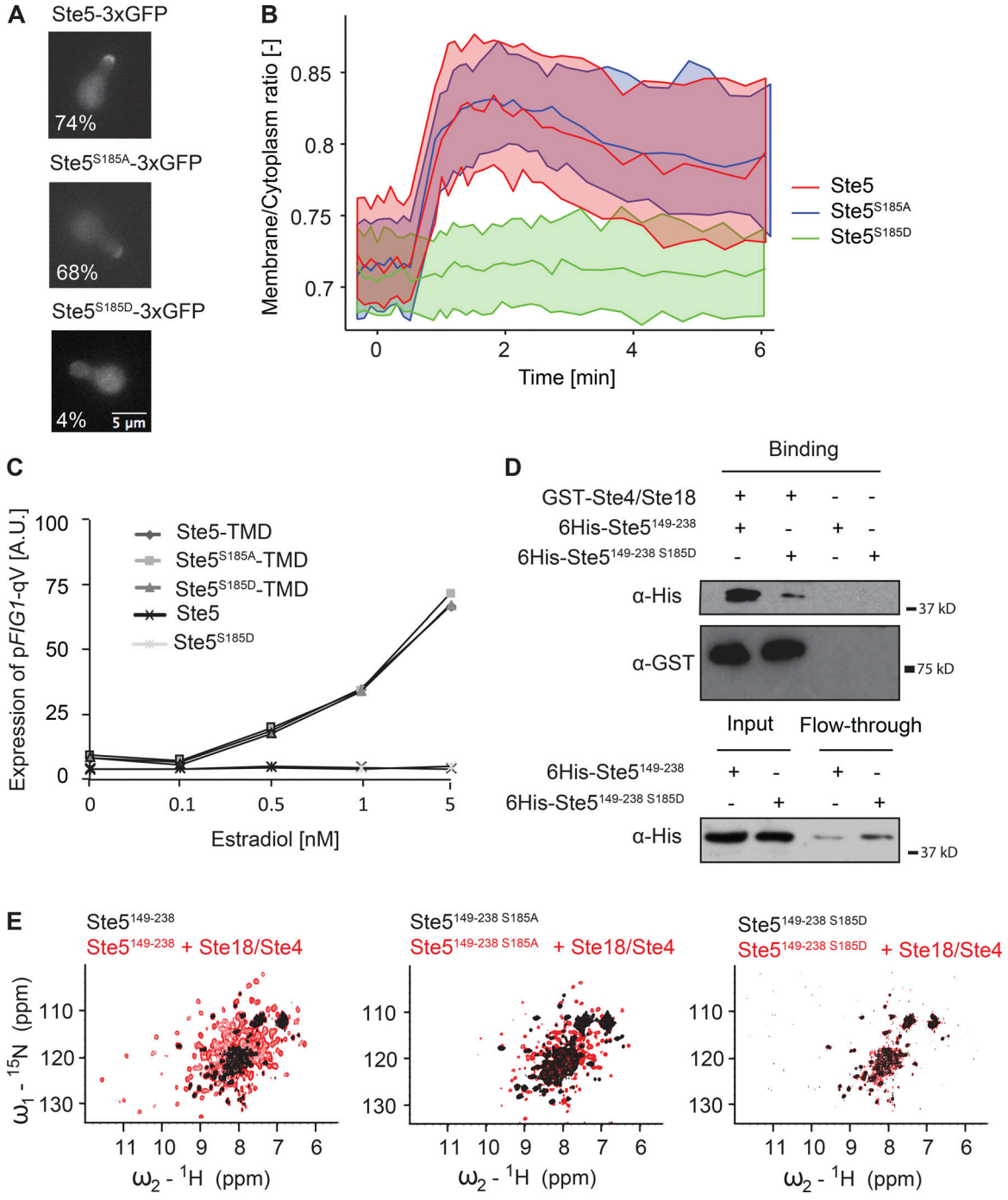

Figure 4. **Phosphorylation of serine 185 interferes with membrane recruitment of Ste5 and prevents Gβγ binding. (A)** The localization of 3xGFP-tagged WT Ste5 (upper panel), Ste5^{S185A} (middle panel), or Ste5^{S185D} (lower panel) expressed in WT cells exposed to α-factor was analyzed by light microscopy. The percentage of cells with accumulated GFP-signal at shmoo tips was quantified by counting ≥100 cells for each strain. **(B)** Recruitment of 3xGFP-tagged WT Ste5, Ste5^{S185A} or Ste5^{S185D} was quantified in single cells at the indicated times upon addition of α-factor (t = 0). The membrane-to-cytoplasmic ratio was calculated using YeastQuant (Pelet et al., 2012) using TMD-mCherry to segment the plasma membrane. The solid line represents the median of the single-cell traces and the shaded area the 25th–75th percentiles. **(C)** FIG1-qV reporter expression was measured by FACS in *ste5Δ* cells expressing from the estradiol-inducible GAL promoter WT Ste5 (diamond), nonphosphorylatable Ste5^{S185A} (square), or phospho-mimicking Ste5^{S185D} (triangle) fused to a TMD and plotted in arbitrary units for different estradiol concentrations. For control, WT Ste5 (x) and Ste5^{S185D} (*) were also expressed without TMD fusion. **(D)** GST-Ste4–Ste18 purified from yeast was immobilized on glutathione-Sepharose beads and incubated in vitro with either 6His-tagged Ste5 WT (Ste5$^{149–238}$) or S185D (Ste5$^{149–238\ S185D}$) RING domains expressed in *E. coli*. Bound and flow-through fractions were collected and analyzed by Western blotting with the indicated antibodies. +, protein added; –, protein omitted. An aliquot of the input fraction controls for the presence of the specified proteins. GST-Ste4–Ste18 preferentially binds to the nonphosphorylated Ste5-RING domain. **(E)** Overlay of [^{1}H, ^{15}N] correlation spectra of WT (left panel), S185A (middle panel), and S185D (right panel) Ste5 RING-H2 domain in free form (black contours) and in complex with Gβγ subunits (red). Ste5 adopts a better-defined fold upon binding Gβγ binding with larger peak dispersion. In contrast to WT and the S185A mutant, the S185D RING-H2 domain fails to interact with Gβγ heterodimers.

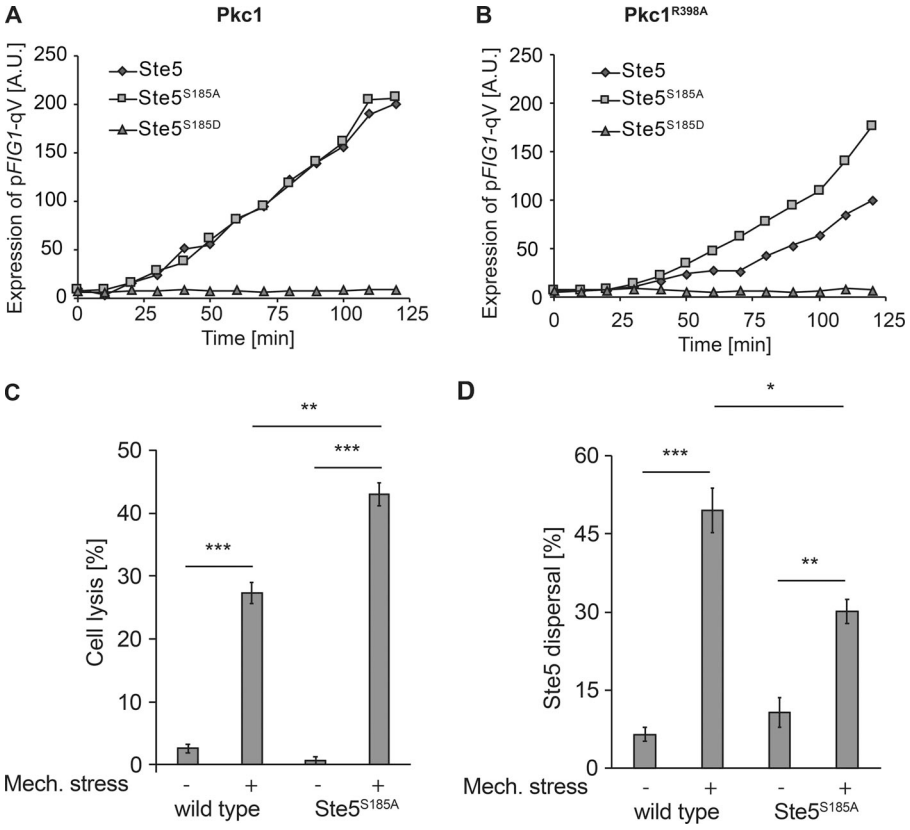

Figure 5. **Pkc1-dependent phosphorylation of Ste5-Ser185 inhibits signaling and prevents lysis during mechanostress. (A and B)** Expression of the FIG1-qV reporter was measured by FACS in *ste5Δ* cells expressing GFP-tagged WT Ste5 (diamond), Ste5^{S185A} (square), or Ste5^{S185D} (triangle) and plotted in arbitrary units at the times after addition of α-factor. The cells were transformed with a plasmid expressing either WT (Pkc1, A) or dominant-active (Pkc1^{R398A}, B) Pkc1 from the inducible GAL1-promoter for 2 h. Expression of Pkc1^{R398A} inhibits pheromone signaling in a Ste5^{Ser185}-dependent manner. **(C)** Cell lysis upon mechanostress in cells expressing WT Ste5 or Ste5^{S185A} mutant was analyze in cells treated as in Fig. 1 A; ≥150 shmooing cells from three independent experiments were analyzed for each condition and are shown as percentage of lysed cells. The error bars indicate SEM, and significance was validated with a *t* test (*, P ≤ 0.05; **, P ≤ 0.01; ***, P ≤ 0.001). **(D)** Dispersal of either tV-tagged WT Ste5 or Ste5^{S185A} from shmoo tips upon mechanostress in cells treated as in Fig. 1 A. Loss of Ste5-tV at shmoo tips was quantified in ≥150 cells from three independent experiments for each condition and is shown as percentage of cells with dispersed Ste5 localization. The error bars indicate SEM, and significance was validated with a *t* test (**, P ≤ 0.01; ***, P ≤ 0.001).

Pkc1-dependent phosphorylation of Ste5 is required to turn off pheromone signaling to prevent lysis during mechanostress and cell–cell fusion

We quantified by FACS analysis the transcriptional induction of the pFIG1-qV reporter in the presence of either WT Pkc1 or a dominant-active mutant (Pkc1^{R398A}). After α-factor exposure in the presence of WT Pkc1, *ste5Δ* cells harboring untagged WT Ste5 or Ste5^{S185A} strongly induced expression from the FIG1 promoter, while cells expressing Ste5^{S185D} did not display induction, even after prolonged exposure (Fig. 5 A). In contrast, upon expression of Pkc1^{R398A}, induction of pFIG1-qV was reduced (Fig. 5 B). Importantly, this reduction was at least partially alleviated in cells expressing the nonphosphorylatable (Ste5^{S185A}) mutant as the only Ste5 copy. We next examined whether Pkc1-mediated crosstalk is physiologically important in vivo. Indeed, α-factor treated *ste5^{S185A}* cells exposed to mechanical stress showed increased cell lysis compared with WT controls (Fig. 5 C), and this defect was accompanied by reduced ability to remove Ste5-tV from shmoo tips (Fig. 5 D). We conclude that phosphorylation of Ste5 in a Pkc1-dependent manner inhibits pheromone signaling, thereby reducing polarized growth at shmoo tips to prevent cell lysis.

Mechanical cell wall stress occurs during the mating response, in particular during cell–cell fusion. To test whether Pkc1-dependent crosstalk prevents cell lysis during mating, we performed quantitative mating assays. Cells expressing the nonphosphorylatable Ste5^{S185A} mutant mated with reduced efficiency compared with WT controls (Fig. 6 A), which could be partially rescued by sorbitol (Fig. S5 D), indicative of a CWI defect. To examine whether this defect results from problems during cell–cell fusion, we designed a microfluidic device to trap mating-competent **a**- and α-cells to visualize the entire mating process and specific marker proteins by fluorescence microscopy in single cells (Fig. 6 B). Lysis during pheromone-induced cell–cell fusion was increased in cells expressing either Ste5^{S185A} or Far1^{3A} (Fig. 6 C). When both mating partners express Ste5^{S185A} and/or Far1^{3A} the lysis phenotype was exacerbated, implying that reduced pheromone signaling at the fusion site is necessary in both mating partners. Concomitantly, the time and position of the first bud emergence in viable zygotes was altered in Ste5^{S185A}-expressing cells (Fig. 6 D), and this cell cycle reentry delay worsened in *ste5^{S185A} far1^{3A}* double mutants. To corroborate these results, we compared Ste5 disappearance from the fusion site in *ste5Δ* cells expressing either GFP-tagged WT or nonphosphorylatable Ste5^{S185A}. As expected, WT Ste5-GFP accumulated at sites of cell–cell contact and rapidly dispersed to the cytoplasm concomitant with cell–cell fusion (Fig. 6 E). However, GFP-Ste5^{S185A} persisted at sites of cell–cell fusion (Fig. 6, F and G), suggesting that phosphorylation of S185 contributes to Ste5 turnover at the fusion site. Taken together, we propose that Pkc1 activated by mechanical stress restricts pheromone signaling during cell–cell fusion at least in part by triggering dissociation of Ste5 and Far1 from the fusion site to facilitate local cell wall remodeling and prevent cell lysis.

Discussion

The scaffolds Ste5 and Far1 comprise important regulatory nodes that spatially and temporally orchestrate yeast mating. While

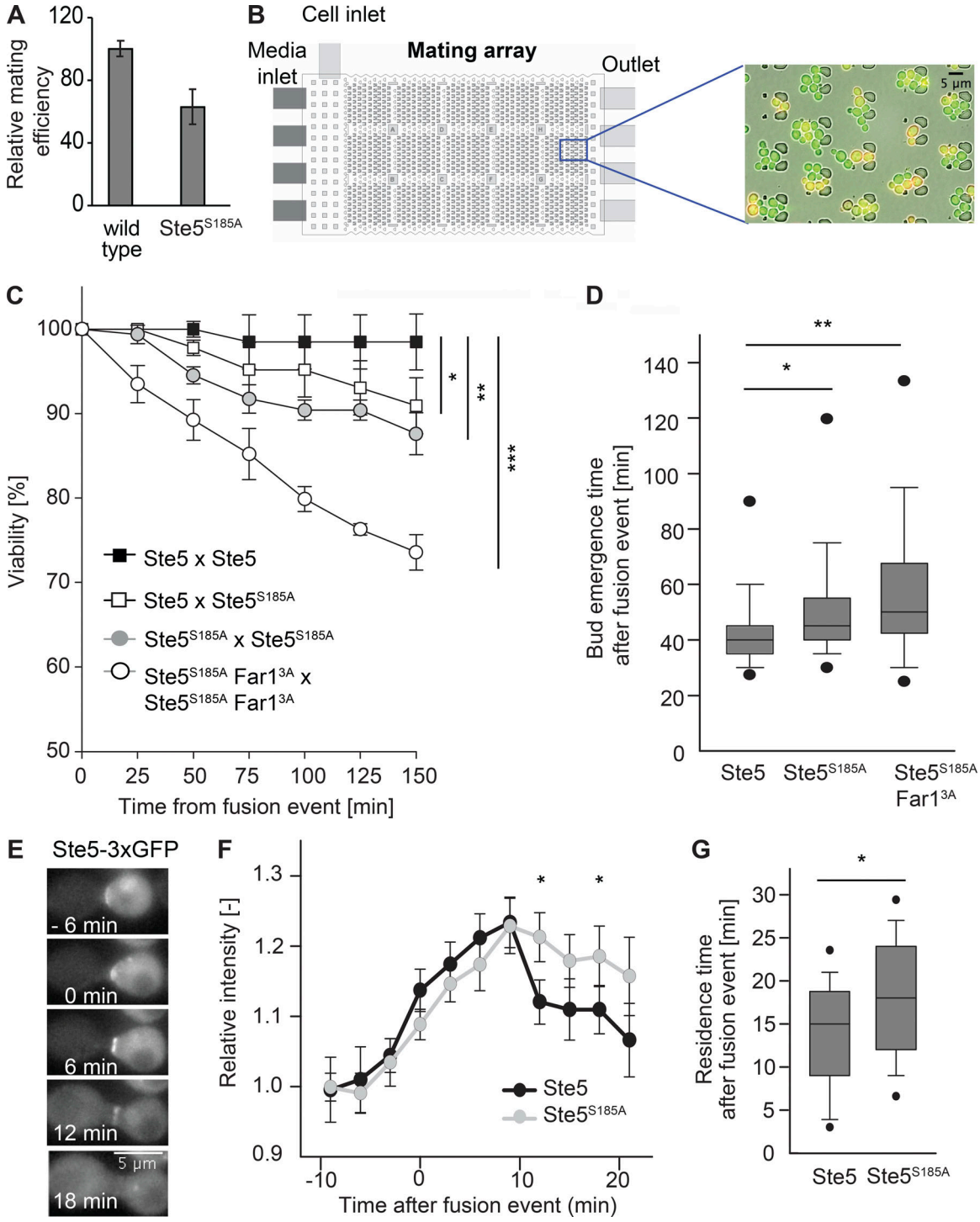

Figure 6. **Pkc1 prevents cell lysis by promoting membrane dissociation of Ste5 and Far1 upon cell–cell fusion. (A)** The relative mating efficiency of *ste5Δ* cells expressing either WT Ste5 or Ste5^{S185A} was measured in media where only diploid cells can grow. The SD was determined from at least three experiments. **(B)** Schematic of the microfluidic device used to observe the mating process. Cells were captured in pockets (magnified inset) and imaged by live-cell microscopy. The pillar array (1,008 traps/array) allows one to trap cells and visualize mating. **(C and D)** Zygotes resulting from the indicated crosses were followed after fusion and scored for cell lysis by microscopy. **(C)** The percentage of viable diploids is plotted as a function of time after cell–cell fusion; ≥100 zygotes from three different experiments were analyzed for each cross. The error bars indicate SD of three independent experiments, and significance was determined for the 150-min time point by a *t* test (*, P ≤ 0.05; **, P ≤ 0.01; ***, P ≤ 0.001). **(D)** Zygotes were assessed for emergence of their first bud after fusion event. Box and whisker plots show median and first and third quartiles, with the outlier 5th and 95th percentiles indicated as symbols (filled circles). Significance was determined by ANOVA and a *t* test (*, P ≤ 0.05; **, P ≤ 0.01). **(E)** 3xGFP-tagged Ste5 expressed in MAT**a** cells was localized by fluorescence microscopy during cell–cell fusion with unlabeled MATα-partners. Images were taken at the indicated times with t = 0 defined when cell–cell contact is detected. Successful cell–cell fusion was monitored by the appearance of GFP-tagged proteins in the unlabeled mating partner. **(F and G)** The levels of 3xGFP-tagged WT Ste5 and Ste5^{S185A} at the site of cell–cell fusion were quantified, and relative intensity with SD compared with the cytoplasmic signal as a function

of time was plotted (F). t = 0 was defined as cell–cell fusion, monitored by the appearance of GFP-tagged proteins in the unlabeled mating partner. Zygotes were assessed for the time of localized GFP residence. The error bars indicate SD of three independent experiments, and significance was determined by a *t* test at the indicated time points (*, P ≤ 0.05). **(G)** Box and whisker plots show median and first and third quartiles, with the outlier 5th and 95th percentiles indicated as symbols (filled circles); ≥70 cells were analyzed, and a *t* test was used to determine significance (*, P ≤ 0.05).

their functions in establishing mating signaling and polarization are comparatively well understood, much less is known about their role in modulating signaling in stressed mating cells. Here, we show that direct phosphorylation of the RING-H2 domains of Ste5 and Far1 regulates their interaction with Gβγ in cells exposed to mechanical stress. Interestingly, this crosstalk mechanism is functionally important both during cell–cell fusion and upon cell wall compression by external mechanical stress. Although the CWI pathway is activated, its MAPK Mpk1 is mostly dispensable for this crosstalk. Instead, we found that Pkc1 triggers removal of Ste5 and probably Far1 from sites of polarized growth, thereby inhibiting pheromone signaling and polarized growth to prevent cell lysis.

Multiple mechanisms and kinases regulate Ste5 membrane association and modulate signaling

Previous work identified several phosphorylation-dependent mechanisms that regulate Ste5 and Far1 activity with altered environmental conditions, and pheromone activation tunes Ste5 output with positive and negative feedback loops. For example, our MS uncovered phosphorylation of four sites near the MAPK-docking site in Ste5, including T287, which was previously proposed to be targeted by Fus3 as part of a negative feedback circuit (Bhattacharyya et al., 2006; Malleshaiah et al., 2010), although this conclusion was recently challenged (Winters and Pryciak, 2019). All four sites are followed by prolines, including S276 located on the same tryptic peptide as T287. It is thus possible that analogous to T287, phosphorylation of these MAPK consensus sites may allosterically contribute to negative feedback regulation in the pheromone-signaling pathway.

Multiple kinases regulate Ste5 membrane association to perturb signaling. It is well established that CDK1 phosphorylates several residues within an amphipathic helix in the N-terminal domain of Ste5 (Strickfaden et al., 2007) and thereby explains why pheromone signaling is restricted to the G1 phase of the cell cycle (Oehlen and Cross, 1994). These and other sites in the PH domain are also phosphorylated by Fus3, constituting a negative feedback mechanism that regulates membrane turnover of Ste5 and tunes down its signaling activity during mating (Repetto et al., 2018). Our analysis identified additional phosphorylation sites on Ste5 and Far1 that conform to the minimal MAPK consensus sites, including T456 located within the Ste5 PH domain. Indeed, mutating T456 to a phospho-mimicking aspartic acid residue ($Ste5^{T456D}$) reduced signaling output (unpublished data), while Ste5 signaling capacity was unchanged when the same site was mutated to a nonphosphorylatable valine residue. Thus, phosphorylation of multiple sites within distinct membrane-binding domains comprises negative feedback that cooperatively modulates the residence time of Ste5 at the plasma membrane. This multisite-phosphorylation mechanism is expected to set a threshold constraining signaling activity during mating and preventing Ste5 activation under conditions of high CDK1 activity in the cell cycle.

Pkc1 directly phosphorylates Ste5 S185 in the RING-H2 domain and prevents membrane localization by interfering with Gβγ binding

We identified a novel mechanism for how single-site phosphorylation regulates Ste5 membrane turnover in response to mechanical stress. Indeed, mutating serine 185, located in its RING-H2 domain, to the phosphomimetic aspartic acid directly interferes with Gβγ binding, suggesting that phosphorylation is sufficient to disrupt binding and that a similar mechanism may regulate the polarity scaffold Far1. Consistent with this notion, cells expressing $Ste5^{S185D}$ are unable to signal, and the mutant protein is not recruited to the plasma membrane upon pheromone exposure. This signaling defect can be rescued by artificially tethering the $Ste5^{S185D}$ mutant protein to the plasma membrane, demonstrating that the defect is mainly caused by abolished membrane recruitment. Mechanistically, phosphorylation of S185 within the RING-H2 domain may directly prevent Gβγ binding through electrostatic repulsion. Alternatively, NMR analysis revealed an induced-fit mechanism such that upon Gβγ binding, the Ste5 RING-H2 domain adopts a fold that may include an asymmetric dimerization typical for many known RING-H2 E3 ligases (Yudina et al., 2015; Sanchez et al., 2016). S185 phosphorylation may thus interfere with folding and prevent stabilization of the active conformation. Irrespective of the underlying mechanism, phosphorylation of a single site in the RING-H2 domain of Ste5 blocks its signaling function by interfering with Gβγ binding and thus membrane association. While we do not know the stoichiometry of S185 phosphorylation, this regulatory mechanism could function as an on/off switch at shmoo tips rapidly activated during stress responses rather than a global tunable rheostat typically observed for multisite phosphorylation.

Although we were unable to confirm that S185 phosphorylation depends on Pkc1 or mechanical stress in vivo, several lines of evidence suggest that the RING-H2 domain of Ste5 is directly phosphorylated by Pkc1. First, Pkc1 is activated by mechanical stress, and its activity is required to prevent cell lysis by inhibiting Fus3. Second, Pkc1 and Ste5 colocalize at shmoo tips and the site of cell–cell fusion. Third, Ste5 physically interacts with Pkc1, and this interaction increases during prolonged α-factor treatment. Fourth, S185 is phosphorylated by purified Pkc1 in vitro and S185 is phosphorylated in vivo in α-factor–treated cells. Finally, expression of a constitutively activate Pkc1 mutant interferes with FIG1-qV reporter expression in WT cells but much less in $ste5^{S185A}$ mutant strains, and $ste5^{S185A}$ cells are prone to lyse upon mechanical stress and during cell–cell fusion. Taken together, these data suggest that mechanical stress activates Pkc1, which in turn phosphorylates Ste5 on S185 located within

the RING-H2 domain, thereby blocking its Gβγ-mediated membrane recruitment. While Pkc1 likely down-regulates Ste5 activity in response to mechanical stress, it is possible that other kinases similarly use S185 phosphorylation to inhibit pheromone signaling in response to other intrinsic or extrinsic stress conditions.

Pkc1-mediated inactivation of the pheromone-response pathway is required to prevent cell lysis of cells experiencing external or intrinsic mechanical stress

Cell wall stress activates the CWI signaling pathway, which through Pkc1 and its downstream MAPK Mpk1 rapidly prevents actin polarization and polarized growth (Levin, 2011). Mpk1 also regulates the production and assembly of cell wall components such as chitin β-1,3-glucan and several mannoproteins and thus repairs and strengthens the protective cell wall (Roemer et al., 1994). Recent evidence demonstrates that compressive mechanical stress is sensed by Mid2, which in turn rapidly triggers Pkc1 activation to prevent cell lysis during bud emergence and shmoo formation (Mishra et al., 2017). As expected, pheromone-treated *mpk1Δ* cells are prone to lyse upon mechanical stress. However, our results identified an additional, Mpk1-independent function of Pkc1 in regulating the scaffolds Ste5 and Far1 to tune down pheromone signaling. Indeed, Pkc1 triggers removal of Ste5 from shmoo tips, resulting in reduced Fus3 activity. Mechanostress-induced cell lysis of shmooing cells in the absence of Pkc1 activity is prevented by simultaneous inactivation of Fus3. Thus, analogous to Hog1 in response to high osmolarity (Hall et al., 1996), this crosstalk mechanism is functionally important to protect cells from lysis when exposed to mechanical stress.

Pkc1-mediated Ste5 phosphorylation also comprises an intrinsic regulatory mechanism temporally and spatially orchestrating mating. Indeed, in cell–cell fusion, cells have to locally break down their cell wall to allow membrane fusion (Merlini et al., 2013). These two steps are carefully coordinated, as early engagement could trigger osmotic shock and lysis. How proper timing is established remains unknown, but it has been proposed that cell fusion depends on Fus3 activity and requires particularly high levels of pheromones (Brizzio et al., 1996). In addition, cells engage an unknown protection pathway that results in Pkc1 activation to antagonize cell wall reorganization if cells are osmotically unstable or morphology is disrupted (Philips and Herskowitz, 1997). Using a microfluidic chip, we found that this Pkc1-dependent protection mechanism involves inhibition of pheromone signaling and polarized growth by inactivation of Ste5 and Far1. Pheromone signaling down-regulation may be necessary to allow efficient cell wall repair and reestablish osmobalance before the fusion process can continue. In absence of this mechanism, sustained Fus3 and Cdc24 activity with cell wall stress at the site of cell fusion may uncouple polarized growth from cell wall remodeling, ultimately leading to cell lysis. Alternatively, removal of Ste5 and Far1 from the fusion site may directly impact the fusion machinery. Indeed, Ste5 physically interacts with the membrane protein Fus1 (Nelson et al., 2004), which is required for polarization and efficient cell wall remodeling during the cell–cell fusion process. Taken together, our data suggest that crosstalk between Pkc1 and the pheromone signaling pathway coordinates cell–cell fusion and prevents untimely cell wall remodeling during the process.

Materials and methods

Yeast strains, plasmids, and growth conditions

All yeast strains and plasmids are listed in Tables 1 and 2, respectively. Yeast strains are derivatives of BY4741 (Brachmann et al., 1998) or w303. Gene fusions were generated by homologous recombination–based replacement of the endogenous gene, and expressed from their endogenous promoter unless otherwise indicated. Strains for all experiments were grown in synthetic media (0.17% yeast nitrogen base, 2% glucose, 0.5% NH_4-sulfate, and amino acids). α-Factor (Genscript) was used at 2.7 µM concentration, unless indicated otherwise. To induce expression of proteins from the *GAL1*-promoter, 2% galactose was added for 2 h unless indicated otherwise to cells growing logarithmically in media containing 2% raffinose were added for 2 h.

Protein extracts and Western blotting

Protein extracts were prepared from TCA-fixed cells. TCA pellets were resuspended in 2× urea buffer (62.5 mM Tris, pH 6.8, 10% glycerol, 4% SDS, 5% β-mercaptoethanol, 8 M urea, and bromophenol blue) and vortexed 3 min at 4°C with 0.5-mm glass beads. After boiling, samples were analyzed using standard SDS-PAGE and Western blotting procedures. Antibodies used included α-GFP (11 814 460 001; Roche), α-PGK1 (A6457; Invitrogen), α-GST (G1160; Sigma), α-His (H1029; Sigma), α-me3K9H3 (NBP1-30141; Novus), GαR-HRP (170-6515; Biorad), and GαM-HRP HRP (170-6516; Biorad). The signal was visualized using SuperSignal West Pico PLUS (1863096; Thermo Fisher Scientific) and film (SuperRX, 47410 19236; Fuji). Protein extracts for in vitro kinase assays were prepared as follows: exponentially growing yeast cells were lysed by freezer milling (Kraft et al., 2012) and the powder was resuspended in PBS buffer with 3 mM EDTA, Roche Inhibitor Tablet, Sigma Inhibitors of yeast proteases, 0.5% Triton X-100, and 2 mM DTT. The extract was cleared by centrifugation at 235,000 ×*g*, and equal amounts of the supernatant were used for the in vitro kinase assays.

Microscopy, microfluidics, and image analysis

Images were acquired on fully automated inverted epifluorescence microscopes (Ti-Eclipse; Nikon) in an incubation chamber set to 30°C with Nikon CFI Plan Apochromat 60×, NA 1.4 objective, a Hamamatsu ORCA Flash 4.0 camera and Micromanager 1.4, and appropriate excitation and emission filters. A motorized XY-stage and piezo drive was used to acquire Z-stacks and multiple fields of view per time point.

Crosstalk between mechanostress and pheromone signaling was studied using a microfluidic device that can apply compressive mechanical stress (Mishra et al., 2017). MAT**a** cells growing in mid-log phase were treated with 2.7 µM α factor for 100 min and loaded in the microfluidic chip, which was precoated with 1 mg/ml Con A. Where appropriate, cells were pretreated for 15 min with the solvent DMSO or, as indicated,

Table 1. **Yeast strains**

Name	Genotype	Source	Used in figure
BY4741	MAT**a** *his3Δ1*; *leu2Δ0*; *met15Δ0*; *ura3Δ0*	OpenBiosystems	Parental
w303	leu2-3,112 trp1-1 can1-100 ura3-1 ade2-1 his3-11,15	Lab collection	Parental
yRM119	BY4741 Prps2-Ste7DS(1-30)-2xNLS(9SP)-Cherry::*URA3* hta2Δ::Hta2-CFP::*HIS3*	Durandau et al., 2015	Fig. 1, D and E; and Fig. S1 A
yRM120	BY4741 *pkc1Δ*::PKC1-GFP-*HIS3MX6* *ura3Δ*::TMD-dCherry	Mishra et al., 2017	Fig. S2 A
yRM230	BY4741 Bni1-qV::*URA3* TMD-dCherry::*LEU2* *fus3Δ*::Fus3-as1::*HIS3*	Mishra et al., 2017	Fig. 1 F
yRM242	w303 ste5Δ::*ADE2*, STE5-tV::*LEU2*	This study	Fig. 1, A–C, G, and H; Fig. 5, C and D; and Fig. S2, C–F
yRM243	w303 *ste5Δ*::*ADE2*, *ste5Δ*:: Ste5^{S185A}-tV::*LEU2*	This study	Fig. 5, C and D
yRM244	yRM242 *mpk1Δ*::kanMX	This study	Fig. 1, G and H; and Fig. S2 C
yRM251	yRM242 empty - *TRP1*	This study	Fig. S2 G
yRM252	yRM242 *BCK1-20*::*TRP1*	This study	Fig. S2 G
yRM253	BY4741 *gat1Δ*::GAT1-GFP-*HIS3MX6*	Collection	Fig. S1 B
yRM254	BY4741 *sfp1Δ*::SFP1-GFP-*HIS3MX6*	Collection	Fig. S1 C
WR232	w303 SILAC STE5-HTBn::*hphMX*, lys1Δ::*kanMX*, arg4Δ::*kanMX*, *CAN1*	This study, W303 SILAC background described in Reiter et al., 2012	Figs. 2 A and S3
WR254	w303 SILAC FAR1-HTBeaq::*hphMX*, lys1Δ::*kanMX*, arg4Δ::*kanMX*, *CAN1*	This study	Figs. 2 A and S3
WR484	w303 SILAC STE5-HTBn::*hphMX*, FAR1-HTBeaq::*hphMX*, lys1Δ::*kanMX*, arg4Δ::*kanMX*, *CAN1*	This study	Figs. 2 A and S3
WR658	w303 SILAC Ste5HTBnp::*hphMX*, ste7Δ::*HIS3*, lys1Δ::*kanMX*, arg4Δ::*kanMX*, *CAN1*	This study	Figs. 2 A and S3
WR725	w303 Ste5-HTBn::*hphMX*, ste7Δ::*HIS3*, ste12Δ::*kanMX*, sst2Δ::*natMX*	This study	Figs. 2 A and S3
WR800	w303 SILAC STE5-HTB::*hphMX*, stl2Δ::*kanMX*, lys1Δ::*kanMX*, arg4Δ::*kanMX*, *CAN1*	This study	Figs. 2 A and S3
JA596	w303 STE5-HKMT-myc::*LEU2*; PKC1-protA-H3-HA::*URA3*; *bar1Δ*	This study	Fig. 2 G
YFD230	w303 ste5Δ::*ADE2*	This study	Parental
yFD702	w303 ste5Δ::*ADE2* Ste5^{S185D}-3GFP::*URA3*	This study	Fig. 3, A and B
ySP85	w303 ste5Δ::*ADE2* Ste5-3GFP::*URA3*	This study	Fig. 3, A and B
ySP86	w303 ste5Δ::*ADE2* Ste5^{S185A}-3GFP::*URA3*	This study	Fig. 3, A and B
ySP296	w303 ste5Δ::*ADE2* Fig1qV::*LEU2*	This study	Parental
ySP309	w303 Fig1qV::*LEU2* ADGEV::*TRP1*	This study	Parental
ySP323	w303 ste5Δ::*ADE2* pRPS2-mCherry-TMD::*HIS3*	This study	Fig. 4 B and Fig. 6, B and E–G
ySP331	w303 Hta2-mCherry::*URA3* Mpk1-GFP::*HIS3*	Lab collection	Fig. S2 B
ySR8	w303 ste5Δ::*ADE2* Fig1qV::*LEU2* Ste5::*HIS3*	This study	Fig. 3 C; Fig. 5, A and B; and Fig. S5, A and C
ySR112	w303 ste5Δ::*ADE2* Fig1qV::*LEU2* Ste5^{S185A}::*HIS3*	This study	Fig. 3, C and B; Fig. 5, A and B; and Fig. S5, A and C
ySR116	w303 ste5Δ::*ADE2* Fig1qV::*LEU2* Ste5^{S185D}::*HIS3*	This study	Fig. 3 C; and Fig. 5, A and B
yBH56	BY4741 far1Δ::Far1-HA-2xStrp::Ca*URA3*	This study	Figs. 3 D and S3
yBH80	BY4741 far1Δ::Far1$^{3A\ S208S210S211}$-HA-2xStrp::Ca*URA3*	This study	Fig. 3 D
yBH90	BY4741 far1Δ::Far1$^{3E\ S208S210S211}$-HA-2xStrp::Ca*URA3*	This study	Fig. 3 D
L40	AOP-*HIS3*::*LYS2* LexAOP-LacZ::*URA3* *his3Δ* *leu2Δ* *trp1Δ* *ade2Δ*	Lab collection	Fig. S5, A and B
yIS153	W303a TMD-cherry-pRPS2::*LEU2* *far1Δ*::Far1$^{3A\ S208S210S211}$::*URA3* *ste5Δ*::Ste5^{S185A}::*HIS3*	This study	Fig. 6, C and D
yIS155	w303a TMD-cherry-pRPS2::*LEU2* *far1Δ*::Far1::*URA3* *ste5Δ*::Ste5^{S185A}::*HIS3*	This study	Fig. 6, C and D
yIS156	w303a TMD-cherry-pRPS2::*LEU2* *far1Δ*::Far1::*URA3* *ste5Δ*::Ste5::*HIS3*	This study	Fig. 6, C and D

Table 1. **Yeast strains (*Continued*)**

Name	Genotype	Source	Used in figure
yIS158	w303alpha *far1Δ*::Far1::*URA3 ste5Δ*::Ste5::*HIS3*	This study	Fig. 6, C and D
yIS159	w303alpha *far1Δ*::Far1$^{3A\ S208S210S211}$::*URA3 ste5Δ*::Ste5^{S185A}::*HIS3*	This study	Fig. 6, C and D
yIS163	w303alpha *far1Δ*::Far1::*URA3 ste5Δ*::Ste5^{S185A}::*HIS3*	This study	Fig. 6, C and D

with cercosporamide (7.5 µM; Merck) or NaPP1 (5 µM; Tocris Bioscience). Subsequently, mechanostress (7 psi pressure) was applied, and the cellular response was assessed using bright-field as well as fluorescence microscopy. Z-stacks of images were acquired for fluorescent reporters, and the images were analyzed on maximum intensity projections.

Cell viability was assessed using 0.025% trypan blue staining or loss of fluorescence after 30 min of mechanostress. For quantification, redistribution of Ste5-tV or Pkc1-GFP away from shmoo tips within 30 min of mechanopressure was scored as Ste5 or Pkc1 dispersal, respectively. Specifically, the intensities of 4 × 4 pixels (16 pixels square) in the shmoo and brightest area elsewhere were compared and scored as "dispersed" when the reduction at the shmoo area was reduced more than the control area. The number of cells that dispersed Ste5 or Pkc1 from shmoo tips within 30 min of applying mechanical pressure was compared with the number of cells that failed to do so. The Ste5 dispersal was analyzed for cells after induction of Pkc1^{K398A} expression by 2% galactose in 96-well plates. In these experiments, cells with pronounced enrichment of Ste5-tV at shmoo tips were monitored every 10 min, and cells that lost Ste5-tV from shmoo tips within 2 h after addition of 2% galactose were scored manually as cells with Ste5 dispersal. Loss of Ste5-tV from shmoo tips was further confirmed by loss of polarized growth. In experiments involving NaPP1-mediated rescue of cell lysis, cells that had Ste5-tV enriched at shmoo tips but lost total fluorescence and changed bright-field contrast within 30 min of mechanostress were scored as dead cells. Cells with mating protrusions after 100 min of pheromone treatment were counted as shmooing cells.

Fus3 activity was monitored using the SKARS as described previously (Durandau et al., 2015). Briefly, cells displaying cytosolic localization of the reporter after pretreatment with α factor were monitored for 30 min under mechanostress

Table 2. **Plasmids**

Name	Description	Source	Used in figure
pNVT-ST-149–238	6His-Ste5-RING-H2$^{149–238}$	Walczak et al., 2014	Fig. 2, B–D and F; Fig. 4, D and E; and Fig. S4
pNVT-ST-149–238 S185A	6His-Ste5-RING-H2$^{149–238\ S185A}$	This study	Figs. 2 E, 4 E, and S4
pNVT-ST-149–238 S185D	6His-Ste5-RING-H2$^{149–238\ S185D}$	This study	Fig. 4, D and E
pNVT-FR-RING-H2	6His-Far1-RING-H2$^{173-261}$	This study	Fig. 2 B
pMG270	pRD53 GAL1 PKC^{R398A}	Collection	Fig. 5 B and Fig. S2, D–F
pMG269	pRD53 GAL1 PKC^{K853R}	Collection	Fig. 1 C
pGADXP	2 µm LEU2 ADH1pr GAL4 AD	Lab collection	Fig. S5, A and B
pBH13	lexA DBD HA-Far1$^{174–285}$	This study	Fig. S5, A and B
pBH14	GAL4 AD HA-Ste4		Fig. S5, A and B
pBH65	lexA DBD HA-Far1$^{174–285\ 3A\ S208S210S211}$	This study	Fig. S5, A and B
pBH67	lexA DBD HA-Far1$^{174–285\ 3D\ S208S210S211}$	This study	Fig. S5, A and B
pSP151	pRS316 endo-Ste5^{S185A}-3xGFP	This study	Fig. 4, A and B; and Fig. 6, F and G
pSP167	pRS303 pGAL1-Ste5^{S185D}-TMD	This study	Fig. 4 C
pSP169	pRS303 pGAL1-Ste5^{S185A}-TMD	This study	Fig. 4 C
pSP174	pRS316 endo-Ste5^{S185D}-3xGFP	This study	Fig. 4, A and B
pSP175	pRS316 endo-Ste5-3xGFP	This study	Fig. 4, A and B; and Fig. 6, E–G
pSP186	pRS303 endo-Ste5-13myc	This study	Fig. 4 C
pSP188	pRS303 endo-Ste5^{S185D}-13myc	This study	Fig. 4 C
pSP193	Msn2p-NLS-GFP (pPKI-NESMsn2p(567–704)-GFP) LEU2	Görner et al., 2002	Fig. S1 D
pFD344	pRS303 pGAL1-Ste5-TMD	This study	Fig. 4 C
pFD532	GAL1-GST-Pkc1 *URA3* (YBL105C)	Collection	Fig. 2 B
pFD720	pRS426 pGAL1-GST-Ste18–Ste4	This study	Fig. 4, D and E

conditions. Cells that showed enrichment of the reporter in the nucleus when subjected to pressure were scored as Fus3-inhibited cells, while cells that lysed and/or failed to enrich the reporter in the nucleus were scored as Fus3-active cells. In the lysed or protected cells, determined by the integrity of the nucleus (Hta2-CFP signal), Fus3 activity was scored based on SKARS localization. Cells that have SKARS in the cytosol before lysis or during 30 min of mechanostress in protected cells were scored as cells with high Fus3 activity. At least three independent experiments were quantified, with >50 cells analyzed for each condition. Error bars indicate SEM.

Microscopy was performed on the 96-well plates coated with 1 mg/ml Con A (Sigma) when a microfluidic platform was not used. To show that cercosporamide treatment fails to inhibit Fus3, WT cells expressing the Fus3 SKARS were allowed to adhere onto Con A–coated 96-well plates, and DMSO or drugs were applied with or without α factor for the indicated time. For assessing PKA and TORC1 activity, cells expressing GFP-tagged Gat1 or Sfp1 were treated with DMSO, 7.5 µM cercosporamide, or 200 nM rapamycin (LC Laboratories). Moreover, WT cells harboring the PKA reporter Msn2-NLS-GFP (Görner et al., 2002) were treated with DMSO or 7.5 µM cercosporamide or subjected to glucose starvation for 60 min. The localization of the GFP reporter was monitored microscopically every 10 min for 60 min. Note that the plates were not coated with Con A while monitoring Msn2-NLS-GFP dynamics.

Cell orientation assays in pheromone gradients were performed in homemade microfluidic gradient chips as described previously (Hegemann et al., 2015). Experimental cells were mixed with unlabeled WT control cells to internally control for gradient stability. For mating assay, MAT**a** and MATα cells grown in exponential phase were mixed before the experiment and immediately loaded into the chip. All microfluidics devices (gradient and mating) were produced by soft lithography and the detailed process of wafer fabrication, polydimethylsiloxane baking, and bonding process were done as described previously (Lee et al., 2012). The height of the cell culture chamber in the mating chips (5 µm) is similar to that of yeast cells ensuring an identical focal plane to image cell mating and fusion for microscopy during the entire mating process. We continuously provide fresh media with very mild flow (<0.2 µl/min), and the cells are trapped within close proximity so that they can efficiently mate with each other.

Automated image analysis was performed using YeastQuant software on raw images (Pelet et al., 2012) running in MATLAB. For Fig. 4 B, the Z-stack of images (13 steps with 0.225 µm distance) are projected using summation intensity and analyzed using Fiji (Schindelin et al., 2012). Yeast cell mating events were monitored by time-lapse microscopy, successively capturing images. The moment of cell death was identified by the sudden shrinkage of the cell body. Cell viability was defined as the ratio of the total number of mating pairs and cell death events.

Flow cytometry

Saturated overnight cultures in synthetic media were diluted and grown to early log phase (OD_{600} 0.4). Where appropriate, genes under the *GAL1* promoter were induced by addition of galactose to a final concentration of 2%. For the estradiol induction, strains containing the ADGEV constructs were treated with the indicated concentration of estradiol for 2 h. The pheromone response pathway was activated by the addition of 2.7 µM α-factor. Protein translation was stopped at the indicated times by the addition of cycloheximide (0.1 mg/ml). Fluorescence intensity of 10,000 cells was measured by FACS (FACSCalibur; 488 nm excitation 530 nm emission) 3 h after pathway induction. Customized MATLAB scripts were used to analyze the data.

Yeast two-hybrid and quantitative β-galactosidase assays

The two-hybrid assays were performed essentially as described previously (Möckli and Auerbach, 2004). Briefly, for each interaction pair and controls, several colonies were grown to an OD_{600} of 0.5–0.8. One absorbance unit of yeast cultures was pelleted, and cells were lysed, resuspended in 20 µl water, and then transferred to a transparent flat-bottom 96-well plate. 100 µl PXG buffer containing Bluo-gal (Invitrogen) was added, and the absorbance at 420 nm was measured with a flatbed scanner. Images were analyzed using ImageJ (National Institutes of Health).

MS analysis

Histidine-biotin tandem affinity purifications are based on methods described elsewhere (Tagwerker et al., 2006; Reiter et al., 2012), with the following modifications. Cells expressing either Ste5 C-terminally tagged with a modified HTB tag (HTBn: 12xHis-tag and two additional TEV cleavage sites) or HTBeaq-tagged Far1 (Reiter et al., 2012) were grown to mid-logarithmic phase (OD_{600} = 0.6–0.9), treated with 100 nM α-factor for the times indicated, harvested by filtration, and rapidly deep frozen in liquid N_2. All subsequent steps were performed as previously described. In the case of in-gel digestion, HTB purified proteins bound to Streptavidin-Agarose resin (Thermo Fisher Scientific) were eluted by a 5-min incubation at 95°C in 1× Laemmli buffer. Proteins were separated on Novex Bolt 4–12% Bis-Tris Plus gels (Invitrogen) according to the manufacturer's protocol. Protein bands were visualized using SimplyBlue SafeStain (Invitrogen) and further processed as described previously (Reiter et al., 2013). For Far1-Venus purification, cells were grown to mid-log phase and treated for 2 h with 2.87 µM α-factor. Cells were washed in PBS, rapidly frozen in liquid nitrogen, and later lysed using freezer milling (Kraft et al., 2012). The lysed powder was solubilized in xt3 buffer (10 mM Tris-HCl, pH 7.5, 150 mM KCl, 2 mM $MgCl_2$, 0.1% NP-40, 1 mM DTT, and complete protease inhibitors, with EDTA [Roche], 100 µM PMSF, 1 mM Na_3VO_4, 10 mM $Na_4P_2O_7$, 10 mM NaF, and 10 mM β-glycerophosphate) and centrifuged at 4,500 rpm for 5 min, and the remaining supernatant was centrifuged at 20,000 rpm for 10 min (both at 4°C). The cleared lysate was incubated with GFP-trap beads (Chromototek), washed extensively in xt3, and washed extensively in xt3 without detergent, and finally protein was eluted from beads using 200 mM glycine, pH 2.0. The eluate was neutralized in 1.5 M Tris, pH 9.2, and stored at −80°C before processing for MS analysis. In-solution digestion with trypsin was performed as described previously (Reiter et al., 2012). All tryptic peptides

samples were subjected to a second reduction step, applying 30-min incubation with DTT (160 µg) at 56°C. Enrichment using TiO_2 and MS analysis is based on methods described previously (Reiter et al., 2012). We used a LTQ FT Ultra MS (Thermo Fisher Scientific) and a LTQ Orbitrap Velos (Thermo Fisher Scientific) instrument for phosphorylation site mapping with settings as described previously (Reiter et al., 2012). Gel-purified protein samples were analyzed using a LTQ XL MS instrument (Thermo Fisher Scientific). MS raw files were processed using MaxQuant (Cox and Mann, 2008; Cox et al., 2011) software version 1.5.2.8 using standard settings, except the following modifications. Spectra were searched against the *Saccharomyces* Genome Database database (http://www.yeastgenome.org/) containing 6,717 entries (February 3, 2011) and including a list of 248 common laboratory contaminants as well as reversed versions of all sequences. The enzyme specificity was set to trypsin. A maximum of two missed cleavages was allowed. Phosphorylation of serine, threonine, and tyrosine residues, oxidation of methionine, and deamidation of asparagine was searched as variable modification. For stable isotope labeling using amino acids in cell culture (SILAC)–labeled samples, Lys6 and Arg6 were additionally selected. Carbamidomethylation of cysteine was searched as a fixed modification. A maximum of five modifications per peptide was allowed. The false discovery rate for peptide, protein, and site identification was set to 1%. All files except Exp1 were searched together. Minimum delta score for modified peptides was set to 6. The six raw files of Exp1 were searched separately with the same parameters as described previously (Reiter et al., 2012). The MS proteomics data have been deposited at the ProteomeXchange Consortium (Vizcaíno et al., 2013; http://www.proteomexchange.org) via the Proteomics Identifications (PRIDE) partner repository with the dataset identifier PXD004657.

M-track protein–protein proximity assay

Cells expressing HKMT-myc–tagged Ste5 (bait) and protA-H3–tagged Pkc1 (prey) were grown until mid-log phase; treated with α-factor (0.5 µg/ml final concentration) for 0, 30, and 60 min; and harvested by centrifugation. Protein extraction was performed under denaturing conditions (50 mM Tris/HCl, pH 8, 50 mM sodium phosphate buffer, pH 8, 8 M urea, 0.3 M NaCl, and 0.5% Nonidet P-40) by glass bead lysis. Whole-cell extracts were mixed with 2× urea buffer (62.5 mM Tris, pH 6.8, 10% glycerol, 4% SDS, 5% β-mercaptoethanol, 8 M urea, and bromophenol blue). After boiling, samples were analyzed using standard SDS-PAGE. Histone-H3 Lys 9 trimethylation (me3K9H3) of Ste5-protA-H3 was visualized by Western blot using an antibody recognizing me3K9H3 (NBP 1-30141; Novus Biochemicals). Loading was controlled using an antibody (12CA5) recognizing HA.

Protein purifications, kinase assays, and NMR analysis

Expression and purifications of the proteins used for NMR investigation followed protocols previously described (Walczak et al., 2014). Briefly, His-Z–tagged $Ste5^{149–238}$ was expressed in *E. coli* BL21(DE3) cells that were lysed in binding buffer (500 mM NaCl, 50 mM Tris-HCl, 10% glycerol, 2 mM DTT, pH 8.0, EDTA-free Roche Inhibitor Cocktail tablet, 150 µM PMSF, 100 µM $ZnCl_2$, and 4.5 mM imidazole) and bound to an Ni-NTA column. After washing with increasing amounts of imidazole (20, 60, and 100 mM) in binding buffer, $Ste5^{149–238}$ was eluted with 300 mM imidazole in binding buffer before dialysis into 50 mM Tris-HCl, pH 8.0, and 2 mM DTT. Cleavage of the His-Z tag took place during dialysis using 3C PreCission Protease. Subsequently, $Ste5^{149–238}$ was purified over an S-Sepharose column and dialyzed into NMR buffer (100 mM NaCl, 50 mM Tris-HCl, pH 7.2, and 100 µM $ZnCl_2$).The GST-Ste4–Ste18 heterodimer was expressed in yeast cells that were lysed by freezer milling (Kraft et al., 2012). The lysed powder was dissolved in GST-binding buffer (PBS buffer with 3 mM EDTA, Roche Inhibitor Tablet, Sigma Inhibitors of yeast proteases, 0.5% Triton X-100, and 2 mM DTT), cleared by spinning at 235,000 ×*g* and bound to glutathione-S-transferase resin for 5–6 h. 6His-tagged Ste5 RING-H2 fragments were incubated at 4°C for 1 h on a rotating wheel, the resins washed with NMR buffer, and bound proteins were eluted with urea buffer. For NMR experiments, GST-Ste4–Ste18 was eluted with 40 mM reduced Glutathione and applied to a Superdex 75 size exclusion column using NMR buffer as described above.

The in vitro kinase assays for NMR analysis were performed with 150 µM $Ste5^{149–238}$ (in 250 µl) with either assay buffer (3 mM $MgCl_2$ and 1 mM ATP), 5 µl of PKCα (P61-10G; SignalChem), and 0.5-0.8× of Lipid Activator (L51-39, SignalChem) or 250 µl yeast extract complemented with 5 mM ATP and phosphatase inhibitors. Reaction proceeded immediately at room temperature. Heteronuclear correlation NMR experiments were acquired as previously described (Vuister et al., 1991; Schanda et al., 2005). The spectra were measured on Bruker AvanceIII NMR spectrometers equipped with cryogenically cooled probes. The NMR data were processed with the software TOPSPIN 3.2 (Bruker). For in vitro kinase assays using autoradiography detection, His-Z–tagged Ste5- and Far1-RING-H2 domains were expressed and purified as described above, but not cleaved. GST-Pkc1 was affinity purified from yeast extracts using glutathione-S-transferase resin, and the kinase assays were performed in the presence of γ-P^{32}-ATP as described previously (Drogen et al., 2000).

Quantitative mating assays

The quantitative mating assays were essentially performed as described previously (Chenevert et al., 1994). Briefly, 10^6 of either MAT**a** WT or $Ste5^{S185A}$ cells were mixed with 10×10^6 MATα cells, filtered onto 0.45-µm filters, and incubated on permissive YPD (where indicated containing 0.2 M sorbitol) plates for 60 min. Cells were resuspended and plated on SD plates allowing either only growth of MAT**a** cells or diploids. The total number of colony-forming units was determined. All experiments were performed in triplicate.

Statistical analysis

The results of at least three independent experiments are presented as mean values, and the error bars represent SD or SEM, as indicated in the figure legends. Statistical significance was tested using the two-tailed Student's *t* test in Microsoft Excel, and the results are indicated (***, $P < 0.001$; **, $P < 0.01$; *, $P < 0.05$). In addition, we performed one-way ANOVA followed by post-test comparison (Dunn's method) for the data shown in

Fig. 6, D and G. The results are comparable to the ones from the *t* test, and the differences in the median values among the groups are greater than would be expected by chance.

Online supplemental material

Fig. S1 shows the specificity of cercosporamide toward Pkc1. Fig. S2 shows that Pkc1 activation inhibits the pheromone response. Fig. S3 shows mapping of phospho-sites on Ste5 and Far1. Fig. S4 shows NMR-based in vitro phosphorylation assays. Fig. S5 shows two-hybrid analysis of the Far1-RING-H2 domain with Ste4, ste5^{S185A} mating efficiency and schematic representation of the Ste5 RING-H2 domain structure bound to Gβγ. Table S1 lists confidently assigned phosphorylation sites of Ste5. Table S2 lists confidently assigned phosphorylation sites of Far1.

Acknowledgments

We thank J. Tilma, I. Stoffel, J. Augustine, and the D-BIOL NMR platform for technical assistance, S. Honnappa (Novartis, Basel, Switzerland) and P.M. Pryciak (University of Massachusetts Medical School, Worcester, MA) for plasmids, and D. Hollenstein and M. Hartl for help with MS data analysis. We thank T. Mayor and A. Smith for critical reading of the manuscript and the Ammerer, Wider and Peter laboratories for helpful discussions.

This work was supported by the Christian Doppler Forschungsgesellschaft (W. Reiter and I. Dohnal), the European Commission Seventh Framework Project UNICELLSYS (W. Reiter and I. Dohnal), the ETH (grant ETH-23 10-2; M.J. Walczak), and the Swiss National Science Foundation Marie-Heim Vögtlein fellowship (Z. Yudina). Work in the M. Peter laboratory is supported by a European Research Council award, a Swiss National Science Foundation project grant, ETH, and the National Research Foundation of Korea Global Research Laboratory (NRF-2015K1A1A2033054).

The authors declare no competing financial interests.

Author contributions: F. van Drogen, R. Mishra, S.S. Lee, B. Hegemann, S. Pelet, Z. Yudina, and F. Rudolf performed the yeast, biochemistry, and quantitative microscopy experiments. S.S. Lee and R. Mishra designed and constructed the microfluidic device. F. Rudolf, W. Reiter, I. Dohnal, and G. Ammerer carried out the MS analysis, and M.J. Walczak, G. Wider, A. Binolfi, and P. Selenko performed the NMR experiments. F. van Drogen, R. Mishra, S.S. Lee, B. Hegemann, F. Rudolf, Serge Pelet, G. Wider, G. Ammerer, and M. Peter participated in the experimental design. F. van Drogen, R. Mishra, and M. Peter wrote the manuscript, with critical input from all authors.

Submitted: 31 August 2018
Revised: 23 April 2019
Accepted: 19 June 2019

References

Alvaro, C.G., and J. Thorner. 2016. Heterotrimeric G Protein-coupled Receptor Signaling in Yeast Mating Pheromone Response. *J. Biol. Chem.* 291:7788–7795. https://doi.org/10.1074/jbc.R116.714980

Bhattacharyya, R.P., A. Reményi, M.C. Good, C.J. Bashor, A.M. Falick, and W.A. Lim. 2006. The Ste5 scaffold allosterically modulates signaling output of the yeast mating pathway. *Science.* 311:822–826. https://doi.org/10.1126/science.1120941

Brachmann, C.B., A. Davies, G.J. Cost, E. Caputo, J. Li, P. Hieter, and J.D. Boeke. 1998. Designer deletion strains derived from Saccharomyces cerevisiae S288C: a useful set of strains and plasmids for PCR-mediated gene disruption and other applications. *Yeast.* 14:115–132. https://doi.org/10.1002/(SICI)1097-0061(19980130)14:2<115::AID-YEA204>3.0.CO;2-2

Brent, R. 2009. Cell signaling: what is the signal and what information does it carry? *FEBS Lett.* 583:4019–4024. https://doi.org/10.1016/j.febslet.2009.11.029

Brezovich, A., M. Schuschnig, G. Ammerer, and C. Kraft. 2015. An in vivo detection system for transient and low-abundant protein interactions and their kinetics in budding yeast. *Yeast.* 32:355–365. https://doi.org/10.1002/yea.3063

Brizzio, V., A.E. Gammie, G. Nijbroek, S. Michaelis, and M.D. Rose. 1996. Cell fusion during yeast mating requires high levels of a-factor mating pheromone. *J. Cell Biol.* 135:1727–1739. https://doi.org/10.1083/jcb.135.6.1727

Chenevert, J., N. Valtz, and I. Herskowitz. 1994. Identification of genes required for normal pheromone-induced cell polarization in Saccharomyces cerevisiae. *Genetics.* 136:1287–1296.

Choudhury, S., P. Baradaran-Mashinchi, and M.P. Torres. 2018. Negative Feedback Phosphorylation of Gγ Subunit Ste18 and the Ste5 Scaffold Synergistically Regulates MAPK Activation in Yeast. *Cell Reports.* 23:1504–1515. https://doi.org/10.1016/j.celrep.2018.03.135

Colman-Lerner, A., A. Gordon, E. Serra, T. Chin, O. Resnekov, D. Endy, C.G. Pesce, and R. Brent. 2005. Regulated cell-to-cell variation in a cell-fate decision system. *Nature.* 437:699–706. https://doi.org/10.1038/nature03998

Cox, J., and M. Mann. 2008. MaxQuant enables high peptide identification rates, individualized p.p.b.-range mass accuracies and proteome-wide protein quantification. *Nat. Biotechnol.* 26:1367–1372. https://doi.org/10.1038/nbt.1511

Cox, J., N. Neuhauser, A. Michalski, R.A. Scheltema, J.V. Olsen, and M. Mann. 2011. Andromeda: a peptide search engine integrated into the MaxQuant environment. *J. Proteome Res.* 10:1794–1805. https://doi.org/10.1021/pr101065j

Delarue, M., G. Poterewicz, O. Hoxha, J. Choi, W. Yoo, J. Kayser, L. Holt, and O. Hallatschek. 2017. SCWISh network is essential for survival under mechanical pressure. *Proc. Natl. Acad. Sci. USA.* 114:13465–13470. https://doi.org/10.1073/pnas.1711204114

Dohlman, H.G., and J.E. Slessareva. 2006. Pheromone signaling pathways in yeast. *Sci. STKE.* 2006:cm6. https://doi.org/10.1126/stke.3642006cm6

Drogen, F., S.M. O'Rourke, V.M. Stucke, M. Jaquenoud, A.M. Neiman, and M. Peter. 2000. Phosphorylation of the MEKK Ste11p by the PAK-like kinase Ste20p is required for MAP kinase signaling in vivo. *Curr. Biol.* 10:630–639. https://doi.org/10.1016/S0960-9822(00)00511-X

Durandau, E., D. Aymoz, and S. Pelet. 2015. Dynamic single cell measurements of kinase activity by synthetic kinase activity relocation sensors. *BMC Biol.* 13:55. https://doi.org/10.1186/s12915-015-0163-z

Engelberg, D., R. Perlman, and A. Levitzki. 2014. Transmembrane signaling in Saccharomyces cerevisiae as a model for signaling in metazoans: state of the art after 25 years. *Cell. Signal.* 26:2865–2878. https://doi.org/10.1016/j.cellsig.2014.09.003

Ferrell, J.E. Jr., and K.A. Cimprich. 2003. Enforced proximity in the function of a famous scaffold. *Mol. Cell.* 11:289–291. https://doi.org/10.1016/S1097-2765(03)00055-8

Görner, W., E. Durchschlag, J. Wolf, E.L. Brown, G. Ammerer, H. Ruis, and C. Schüller. 2002. Acute glucose starvation activates the nuclear localization signal of a stress-specific yeast transcription factor. *EMBO J.* 21:135–144. https://doi.org/10.1093/emboj/21.1.135

Hall, J.P., V. Cherkasova, E. Elion, M.C. Gustin, and E. Winter. 1996. The osmoregulatory pathway represses mating pathway activity in Saccharomyces cerevisiae: isolation of a FUS3 mutant that is insensitive to the repression mechanism. *Mol. Cell. Biol.* 16:6715–6723. https://doi.org/10.1128/MCB.16.12.6715

Hegemann, B., M. Unger, S.S. Lee, I. Stoffel-Studer, J. van den Heuvel, S. Pelet, H. Koeppl, and M. Peter. 2015. A Cellular System for Spatial Signal Decoding in Chemical Gradients. *Dev. Cell.* 35:458–470. https://doi.org/10.1016/j.devcel.2015.10.013

Inouye, C., N. Dhillon, and J. Thorner. 1997. Ste5 RING-H2 domain: role in Ste4-promoted oligomerization for yeast pheromone signaling. *Science.* 278:103–106. https://doi.org/10.1126/science.278.5335.103

Kraft, C., M. Kijanska, E. Kalie, E. Siergiejuk, S.S. Lee, G. Semplicio, I. Stoffel, A. Brezovich, M. Verma, I. Hansmann, et al. 2012. Binding of the Atg1/

ULK1 kinase to the ubiquitin-like protein Atg8 regulates autophagy. *EMBO J.* 31:3691–3703. https://doi.org/10.1038/emboj.2012.225

Kreegipuu, A., N. Blom, S. Brunak, and J. Järv. 1998. Statistical analysis of protein kinase specificity determinants. *FEBS Lett.* 430:45–50. https://doi.org/10.1016/S0014-5793(98)00503-1

Lee, S.S., P. Horvath, S. Pelet, B. Hegemann, L.P. Lee, and M. Peter. 2012. Quantitative and dynamic assay of single cell chemotaxis. *Integr. Biol.* 4: 381–390. https://doi.org/10.1039/c2ib00144f

Levin, D.E. 2011. Regulation of cell wall biogenesis in Saccharomyces cerevisiae: the cell wall integrity signaling pathway. *Genetics.* 189:1145–1175. https://doi.org/10.1534/genetics.111.128264

Malleshaiah, M.K., V. Shahrezaei, P.S. Swain, and S.W. Michnick. 2010. The scaffold protein Ste5 directly controls a switch-like mating decision in yeast. *Nature.* 465:101–105. https://doi.org/10.1038/nature08946

Merlini, L., O. Dudin, and S.G. Martin. 2013. Mate and fuse: how yeast cells do it. *Open Biol.* 3:130008. https://doi.org/10.1098/rsob.130008

Mishra, R., F. van Drogen, R. Dechant, S. Oh, N.L. Jeon, S.S. Lee, and M. Peter. 2017. Protein kinase C and calcineurin cooperatively mediate cell survival under compressive mechanical stress. *Proc. Natl. Acad. Sci. USA.* 114:13471–13476. https://doi.org/10.1073/pnas.1709079114

Möckli, N., and D. Auerbach. 2004. Quantitative beta-galactosidase assay suitable for high-throughput applications in the yeast two-hybrid system. *Biotechniques.* 36:872–876. https://doi.org/10.2144/04365PT03

Nelson, B., A.B. Parsons, M. Evangelista, K. Schaefer, K. Kennedy, S. Ritchie, T.L. Petryshen, and C. Boone. 2004. Fus1p interacts with components of the Hog1p mitogen-activated protein kinase and Cdc42p morphogenesis signaling pathways to control cell fusion during yeast mating. *Genetics.* 166:67–77. https://doi.org/10.1534/genetics.166.1.67

Oehlen, L.J., and F.R. Cross. 1994. G1 cyclins CLN1 and CLN2 repress the mating factor response pathway at Start in the yeast cell cycle. *Genes Dev.* 8:1058–1070. https://doi.org/10.1101/gad.8.9.1058

Pelet, S., R. Dechant, S.S. Lee, F. van Drogen, and M. Peter. 2012. An integrated image analysis platform to quantify signal transduction in single cells. *Integr. Biol.* 4:1274–1282. https://doi.org/10.1039/c2ib20139a

Philips, J., and I. Herskowitz. 1997. Osmotic balance regulates cell fusion during mating in Saccharomyces cerevisiae. *J. Cell Biol.* 138:961–974. https://doi.org/10.1083/jcb.138.5.961

Pryciak, P.M., and F.A. Huntress. 1998. Membrane recruitment of the kinase cascade scaffold protein Ste5 by the Gbetagamma complex underlies activation of the yeast pheromone response pathway. *Genes Dev.* 12: 2684–2697. https://doi.org/10.1101/gad.12.17.2684

Reiter, W., D. Anrather, I. Dohnal, P. Pichler, J. Veis, M. Grøtli, F. Posas, and G. Ammerer. 2012. Validation of regulated protein phosphorylation events in yeast by quantitative mass spectrometry analysis of purified proteins. *Proteomics.* 12:3030–3043. https://doi.org/10.1002/pmic.201200185

Reiter, W., E. Klopf, V. De Wever, D. Anrather, A. Petryshyn, A. Roetzer, G. Niederacher, E. Roitinger, I. Dohnal, W. Görner, et al. 2013. Yeast protein phosphatase 2A-Cdc55 regulates the transcriptional response to hyperosmolarity stress by regulating Msn2 and Msn4 chromatin recruitment. *Mol. Cell. Biol.* 33:1057–1072. https://doi.org/10.1128/MCB.00834-12

Repetto, M.V., M.J. Winters, A. Bush, W. Reiter, D.M. Hollenstein, G. Ammerer, P.M. Pryciak, and A. Colman-Lerner. 2018. CDK and MAPK Synergistically Regulate Signaling Dynamics via a Shared Multi-site Phosphorylation Region on the Scaffold Protein Ste5. *Mol. Cell.* 69: 938–952.

Roemer, T., G. Paravicini, M.A. Payton, and H. Bussey. 1994. Characterization of the yeast (1-->6)-beta-glucan biosynthetic components, Kre6p and Skn1p, and genetic interactions between the PKC1 pathway and extracellular matrix assembly. *J. Cell Biol.* 127:567–579. https://doi.org/10.1083/jcb.127.2.567

Sanchez, J.G., J.J. Chiang, K.M. Sparrer, S.L. Alam, M. Chi, M.D. Roganowicz, B. Sankaran, M.U. Gack, and O. Pornillos. 2016. Mechanism of TRIM25 Catalytic Activation in the Antiviral RIG-I Pathway. *Cell Reports.* 16: 1315–1325.

Schanda, P., E. Kupče, and B. Brutscher. 2005. SOFAST-HMQC experiments for recording two-dimensional heteronuclear correlation spectra of proteins within a few seconds. *J. Biomol. NMR.* 33:199–211. https://doi.org/10.1007/s10858-005-4425-x

Schindelin, J., I. Arganda-Carreras, E. Frise, V. Kaynig, M. Longair, T. Pietzsch, S. Preibisch, C. Rueden, S. Saalfeld, B. Schmid, et al. 2012. Fiji: an open-source platform for biological-image analysis. *Nat. Methods.* 9: 676–682. https://doi.org/10.1038/nmeth.2019

Smits, G.J., J.C. Kapteyn, H. van den Ende, and F.M. Klis. 1999. Cell wall dynamics in yeast. *Curr. Opin. Microbiol.* 2:348–352. https://doi.org/10.1016/S1369-5274(99)80061-7

Strickfaden, S.C., M.J. Winters, G. Ben-Ari, R.E. Lamson, M. Tyers, and P.M. Pryciak. 2007. A mechanism for cell-cycle regulation of MAP kinase signaling in a yeast differentiation pathway. *Cell.* 128:519–531. https://doi.org/10.1016/j.cell.2006.12.032

Tagwerker, C., H. Zhang, X. Wang, L.S. Larsen, R.H. Lathrop, G.W. Hatfield, B. Auer, L. Huang, and P. Kaiser. 2006. HB tag modules for PCR-based gene tagging and tandem affinity purification in Saccharomyces cerevisiae. *Yeast.* 23:623–632. https://doi.org/10.1002/yea.1380

Vaga, S., M. Bernardo-Faura, T. Cokelaer, A. Maiolica, C.A. Barnes, L.C. Gillet, B. Hegemann, F. van Drogen, H. Sharifian, E. Klipp, et al. 2014. Phosphoproteomic analyses reveal novel cross-modulation mechanisms between two signaling pathways in yeast. *Mol. Syst. Biol.* 10:767. https://doi.org/10.15252/msb.20145112

van Drogen, F., and M. Peter. 2002. Spa2p functions as a scaffold-like protein to recruit the Mpk1p MAP kinase module to sites of polarized growth. *Curr. Biol.* 12:1698–1703. https://doi.org/10.1016/S0960-9822(02)01186-7

Vizcaíno, J.A., R.G. Côté, A. Csordas, J.A. Dianes, A. Fabregat, J.M. Foster, J. Griss, E. Alpi, M. Birim, J. Contell, et al. 2013. The PRoteomics IDEntifications (PRIDE) database and associated tools: status in 2013. *Nucleic Acids Res.* 41(D1):D1063–D1069. https://doi.org/10.1093/nar/gks1262

Vuister, G.W., R. Boelens, A. Padilla, and R. Kaptein. 1991. Statistical analysis of double NOE transfer pathways in proteins as measured in 3D NOE-NOE spectroscopy. *J. Biomol. NMR.* 1:421–438. https://doi.org/10.1007/BF02192864

Walczak, M.J., B. Samatanga, F. van Drogen, M. Peter, I. Jelesarov, and G. Wider. 2014. The RING domain of the scaffold protein Ste5 adopts a molten globular character with high thermal and chemical stability. *Angew. Chem. Int. Ed. Engl.* 53:1320–1323. https://doi.org/10.1002/anie.201306702

Watanabe, M., C.Y. Chen, and D.E. Levin. 1994. Saccharomyces cerevisiae PKC1 encodes a protein kinase C (PKC) homolog with a substrate specificity similar to that of mammalian PKC. *J. Biol. Chem.* 269: 16829–16836.

Whiteway, M.S., C. Wu, T. Leeuw, K. Clark, A. Fourest-Lieuvin, D.Y. Thomas, and E. Leberer. 1995. Association of the yeast pheromone response G protein beta gamma subunits with the MAP kinase scaffold Ste5p. *Science.* 269:1572–1575. https://doi.org/10.1126/science.7667635

Winters, M.J., and P.M. Pryciak. 2019. MAPK modulation of yeast pheromone signaling output and the role of phosphorylation sites in the scaffold protein Ste5. *Mol. Biol. Cell.* 30:1037–1049. https://doi.org/10.1091/mbc.E18-12-0793

Winters, M.J., R.E. Lamson, H. Nakanishi, A.M. Neiman, and P.M. Pryciak. 2005. A membrane binding domain in the ste5 scaffold synergizes with gbetagamma binding to control localization and signaling in pheromone response. *Mol. Cell.* 20:21–32. https://doi.org/10.1016/j.molcel.2005.08.020

Yamamoto, K., K. Tatebayashi, K. Tanaka, and H. Saito. 2010. Dynamic control of yeast MAP kinase network by induced association and dissociation between the Ste50 scaffold and the Opy2 membrane anchor. *Mol. Cell.* 40:87–98. https://doi.org/10.1016/j.molcel.2010.09.011

Yu, R.C., C.G. Pesce, A. Colman-Lerner, L. Lok, D. Pincus, E. Serra, M. Holl, K. Benjamin, A. Gordon, and R. Brent. 2008. Negative feedback that improves information transmission in yeast signalling. *Nature.* 456: 755–761. https://doi.org/10.1038/nature07513

Yudina, Z., A. Roa, R. Johnson, N. Biris, D.A. de Souza Aranha Vieira, V. Tsiperson, N. Reszka, A.B. Taylor, P.J. Hart, B. Demeler, et al. 2015. RING Dimerization Links Higher-Order Assembly of TRIM5α to Synthesis of K63-Linked Polyubiquitin. *Cell Reports.* 12:788–797. https://doi.org/10.1016/j.celrep.2015.06.072

Zarzov, P., C. Mazzoni, and C. Mann. 1996. The SLT2(MPK1) MAP kinase is activated during periods of polarized cell growth in yeast. *EMBO J.* 15: 83–91. https://doi.org/10.1002/j.1460-2075.1996.tb00336.x

Zuzuarregui, A., T. Kupka, B. Bhatt, I. Dohnal, I. Mudrak, C. Friedmann, S. Schüchner, I.E. Frohner, G. Ammerer, and E. Ogris. 2012. M-Track: detecting short-lived protein-protein interactions in vivo. *Nat. Methods.* 9:594–596. https://doi.org/10.1038/nmeth.2017